AD-753 695

The Calculation of Three-Dimensional Supersonic Flows around Spherically-Capped Smooth Bodies and Wings

Volume 1 theory and application

Northrop Corp.

prepared for

Air Force Flight Dynamics Laboratory

SEPTEMBER 1972

Distributed By:

NTIS

National Technical Information Service
U. S. DEPARTMENT OF COMMERCE

AFFDL-TR-72-91
Volume I

THE CALCULATION OF THREE-DIMENSIONAL SUPERSONIC FLOWS AROUND SPHERICALLY-CAPPED SMOOTH BODIES AND WINGS

Volume I. Theory and Applications

C. W. Chu
S. A. Powers

Northrop Corporation
Aircraft Division

TECHNICAL REPORT AFFDL-TR-72-91, Volume I

September 1972

Air Force Flight Dynamics Laboratory
Air Force Systems Command
Wright-Patterson Air Force Base, Ohio 45433

NOTICE

When Government drawings, specifications, or other data are used for any purpose other than in connection with a definitely related Government procurement operation, the United States Government thereby incurs no responsibility nor any obligation whatsoever; and the fact that the government may have formulated, furnished, or in any way supplied the said drawings, specifications, or other data, is not to be regarded by implication or otherwise as in any manner licensing the holder or any other person or corporation, or conveying any rights or permission to manufacture, use, or sell any patented invention that may in any way be related thereto.

Copies of this report should not be returned unless return is required by security considerations, contractual obligations, or notice on a specific document.

UNCLASSIFIED

Security Classification

DOCUMENT CONTROL DATA - R & D

(Security classification of title, body of abstract and indexing annotation must be entered when the overall report is classified)

1. ORIGINATING ACTIVITY *(Corporate author)*

Northrop Corporation
Aircraft Division
Hawthorne, California

2a. REPORT SECURITY CLASSIFICATION

Unclassified

2b. GROUP

3. REPORT TITLE

THE CALCULATION OF THREE-DIMENSIONAL SUPERSONIC FLOWS AROUND SPHERICALLY-CAPPED SMOOTH BODIES AND WINGS - Volume I

4. DESCRIPTIVE NOTES *(Type of report and inclusive dates)*

Final Report - 1 December 1971 to 3 July 1972

5. AUTHOR(S) *(First name, middle initial, last name)*

Chong-Wei Chu
Sidney A. Powers

6. REPORT DATE	7a. TOTAL NO. OF PAGES	7b. NO. OF REFS
September 1972	~~77~~ 87	11

8a. CONTRACT OR GRANT NO.	9a. ORIGINATOR'S REPORT NUMBER(S)
F33615-72-C-1429	NOR 72-87, Volume I
b. PROJECT NO. 1366	
c.	9b. OTHER REPORT NO(S) *(Any other numbers that may be assigned this report)*
d.	AFFDL-TR-72-91, Volume I

10. DISTRIBUTION STATEMENT

Approved for public release; distribution unlimited.

11. SUPPLEMENTARY NOTES	12. SPONSORING MILITARY ACTIVITY
	Air Force Flight Dynamics Laboratory Wright-Patterson Air Force Base Ohio 45433

13. ABSTRACT

This report describes the theories, the numerical methods and the computer programs developed for determining the inviscid three-dimensional flow about smooth shapes at supersonic speeds. Volume I describes the theoretical and numerical approaches and compares two sample cases with experiment; a blunted 15° cone at 20° angle of attack in helium at $M_\infty = 14.9$, and a 70° slab delta wing at 15° angle of attack in air at $M_\infty = 9.6$. The numerical results are in close agreement with the experimental data, even on the lee side of both bodies where good agreement is not expected.

Volume II is the user's manual for the computer programs and provides the detailed information needed to set up and use the programs. These programs can determine the supersonic flow past smooth blunted bodies for any angle of attack for which the initial value surface remains on the blunted nose. Since the sonic point on a sphere lies between 40 and 50 degrees from the stagnation point, the sphere-body juncture should occur at an angle greater than approximately $(50 - \alpha)$ degrees on the sphere, measured in the body axis system.

The lowest usable Mach number is on the order of 2.0, with lower values attainable by careful attention to the initial value surface solution. There is no computational upper limit on the Mach number. However, above $M_\infty = 7.0$ (approximately) the ideal gas model becomes somewhat inaccurate.

DD FORM 1 NOV 68 1473

Ia.

UNCLASSIFIED

Security Classification

14. KEY WORDS	LINK A		LINK B		LINK C	
	ROLE	WT	ROLE	WT	ROLE	WT
Three-Dimensional Flow Fields						
Characteristics Method						
Supersonic Flow						
Hypersonic Flow						
Steady Flow						
Inviscid Flow						
Fuselage Flow Fields						
Delta Wing						
Blunted Cone						
Reentry Body						
Computational Technique						
Numerical Analysis						

I b

THE CALCULATION OF THREE–DIMENSIONAL SUPERSONIC FLOWS AROUND SPHERICALLY–CAPPED SMOOTH BODIES AND WINGS

Volume I

Theory and Applications

C. W. Chu
S. A. Powers

FOREWORD

This report presents a summary of work performed for the Air Force Flight Dynamics Laboratory, Air Force Systems Command, funded under Contract F33615-72-C-1429. The work was performed by the Aerodynamics Research Department of the Northrop Corporation, Aircraft Division, Hawthorne, California.

This report is divided into two volumes. Volume I discusses the theory and the application, and presents comparisons of the numerical results with experimental data. Volume II discusses the details of the computer programs and how to operate them. For internal control purposes, this report has been assigned the Northrop report number, NOR 72-87.

The work reported herein was begun on December 1, 1971, and the final, operational computer programs were delivered and demonstrated in the period of June 14-16, 1972. In addition to the two authors, Mr. Joe Der, Jr., also of the Aerodynamics Research Department, made significant contributions to this work through his knowledge of computing and computing machinery. Mr. Henry Ziegler did a fine job in the preparation of the final report, and Miss Alberta Hansen made all the line drawings.

Mr. A. B. Lewis was the Air Force Project Engineer. He also made very important contributions to the program, and much of the credit for the back-to-back operation of the two programs must go to him for his suggestions and guidance.

This technical report was submitted by the authors in July 1972, and has been reviewed and approved.

for Alfred B. Draper

Philip P. Antonatos
Chief, Flight Mechanics Division
Air Force Flight Dynamics Laboratory

TABLE OF CONTENTS

LIST OF ILLUSTRATIONS

LIST OF ILLUSTRATIONS (Continued)

LIST OF SYMBOLS

a	local speed of sound
A, B, C	coefficients of quadratic equation for base point location
A_i, B_i, C_i, D_i	coefficients of compatibility relation in difference form
B	shock bluntness
B_B	body bluntness
C	1 - B
G	ratio of $\Delta\eta$'s for successive calculation steps
$\hat{j}$	unit vector in Y direction
l_b, m_b, n_b	direction cosines of body normal
l_s, m_s, n_s	direction cosines of free-stream velocity
L	local coordinate in characteristic direction or a factor for determining base point location
M_∞	freestream Mach number
N	local coordinate orthogonal to L
P, Q, R, S, T	coefficients of conic sections for body description
P	pressure
$\vec{q}$	velocity vector
R	radius of curvature at shock apex or universal gas constant
S, s	entropy or distance around a slab delta wing
t	thickness of a slab delta wing
u, v, w	velocity components in X, Y, Z directions, respectively
X, Y, Z	rectangular coordinates
α, β, γ	body parameters
α	angle of attack
γ	ratio of specific heats
δ	local flow direction angle in IVS program or an angle indicating the position of a bicharacteristic in 3DMoC program
Δ	shock stand-off distance in IVS program or flow deflection angle in 3DMoC program
θ, ψ	flow angles in 3DMoC program
θ	shock angle in IVS program

LIST OF SYMBOLS (Continued)

μ	local Mach angle
ν	0 for two-dimensional flow, 1 for rotationally symmetric flow
ξ, η	curvilinear coordinates
ρ	density
ψ	stream function

SECTION I

INTRODUCTION

The inviscid flow field programs contained within the combined viscid-inviscid flow field program described in Reference 1 have been separated from the overall program, revised extensively and improved in many respects. The logic of these programs has been greatly simplified; unused variables and unnecessary blocks of logic have been removed, and many new developments added. As a result, two computer programs are now available for calculating the inviscid supersonic/hypersonic flow over three-dimensional bodies at angles of attack with a high degree of accuracy and for a modest expenditure of computer time.

The resulting new programs are the Initial Value Surface Program and the Three-Dimensional Method of Characteristics Program. Both are based on the use of an ideal gas with a constant ratio of specific heats. Both programs have been designed to require a minimum of input and to be extremely flexible to use. All development decisions were based on the use of both programs by the Air Force Flight Dynamics Laboratory on the Wright-Patterson Air Force Base CDC 6600 computer; use on other machines may result in some compromises.

The bodies which may be created must have spherical noses and no slope discontinuities, but may have upper and lower flat sections (for example, a slab delta wing). Any angle of attack for which the subsonic region does not extend beyond the spherical nose can be handled.

Volume I discusses the theoretical foundations and the numerical methods while Volume II describes the computer programs and how to use them. The original methods were given in Reference 1; a complete, up-to-date discussion of the basic formulation and the numerical methods is presented here.

SECTION II

BODY DESCRIPTION

Figure 1 shows a complex body shape having a spherical nose and upper and lower flats. In a right-handed coordinate system, the Y-axis is aligned with the body axis. The Z-axis is up and the X-axis spanwise. The nose of the body need not coincide with the origin of the coordinate system.

Three lines serve to define this body shape:

(1) The outer limit of the upper flat

(2) The maximum width line

(3) The outer limit of the lower flat.

In cross section, an ellipse is fitted between line (1) and (2), and another ellipse between (2) and (3). For the case of a blunted cone, (or ellipse) the outer limits of the upper and lower flats lie in the plane of symmetry X = 0.

Each line is described by two functions of Y.

$$Z_1 = P_1 Y + Q_1 + SG_1 \sqrt{R_1 Y^2 + S_1 Y + T_1}$$
$$X_1 = P_4 Y + Q_4 + SG_4 \sqrt{R_4 Y^2 + S_4 Y + T_4}$$
$$Z_2 = P_2 Y + Q_2 + SG_2 \sqrt{R_2 Y^2 + S_2 Y + T_2}$$
$$X_2 = P_5 Y + Q_5 + SG_5 \sqrt{R_5 Y^2 + S_5 Y + T_5}$$
$$Z_3 = P_3 Y + Q_3 + SG_3 \sqrt{R_3 Y^2 + S_3 Y + T_3}$$
$$X_3 = P_6 Y + Q_6 + SG_6 \sqrt{R_6 Y^2 + S_6 Y + T_6}$$

Here P, Q, R, S and T are coefficients of the general conic sections and SG is the sign of the square root. Methods for evaluation of these coefficients are discussed in Appendix I.

No slope discontinuities are permitted in the present program. Since each line may be described by several segments, this slope smoothness requirement translates into:

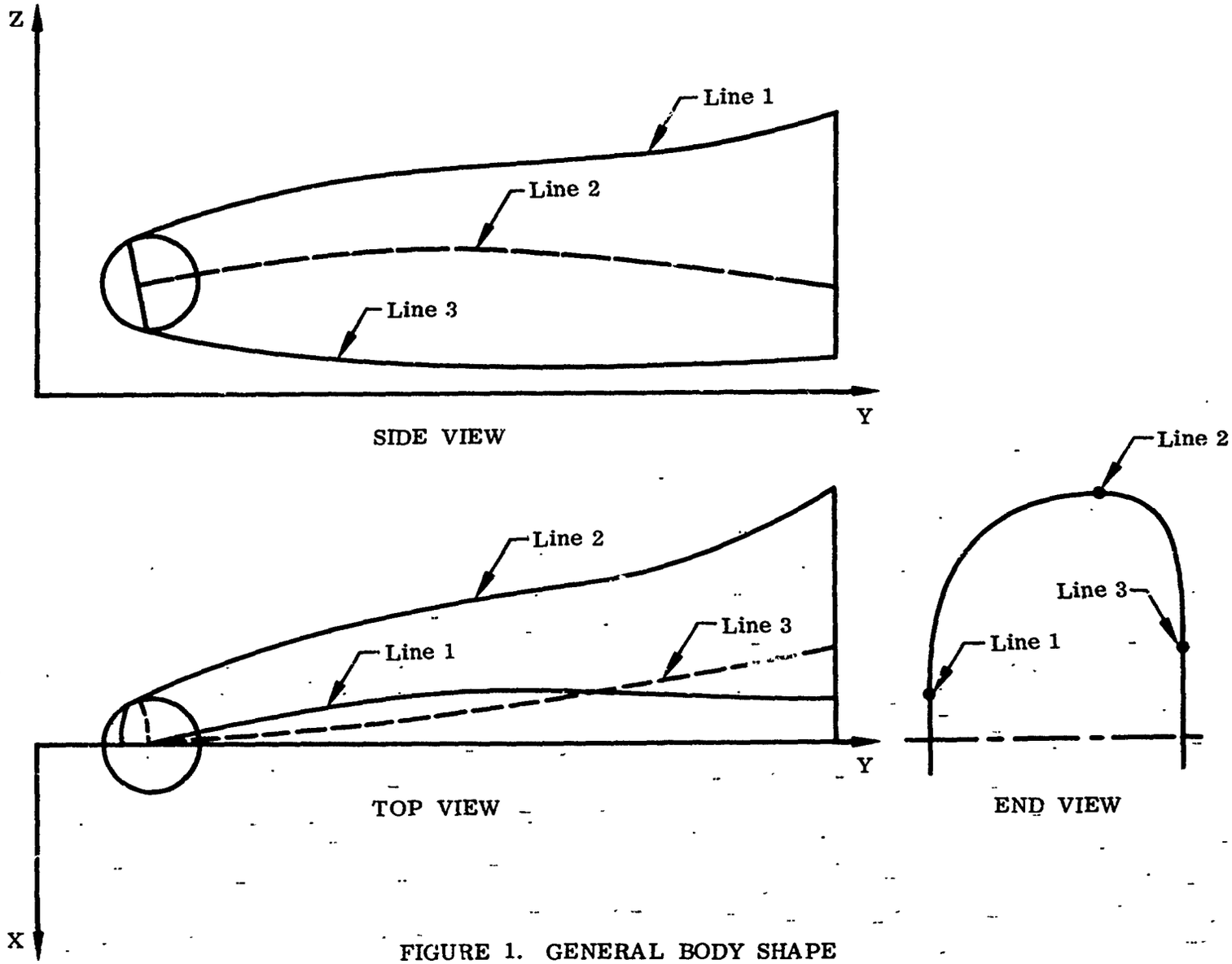

FIGURE 1. GENERAL BODY SHAPE

$\left(\frac{dZ_1}{dY}\right)$ everywhere continuous

$\left(\frac{dX_2}{dY}\right)$ everywhere continuous

$\left(\frac{dZ_3}{dY}\right)$ everywhere continuous

However, $\frac{dX_1}{dY}$, $\frac{dZ_2}{dY}$, and $\frac{dX_3}{dY}$ are not required to be continuous.

Two examples of this body description method are given in Appendix II.

SECTION III

THE INITIAL VALUE SURFACE

The function of the Initial Value Surface (IVS) Program is to provide sufficient data to start the Three-Dimensional Method of Characteristics Program calculation of the supersonic flow field. For reasons of economy, this IVS should be as far downstream as possible in order to compute the largest possible portion of the flow field by means of a rotationally symmetric method. This, of course, implies a minimization of the total computing time required for the total solution.

The present IVS program is a greatly modified version of the old IVS program from Reference 1. Figure 2 compares the old and new approaches.

Since a sphere has no preferential direction, the solution for a sphere at angle of attack can be obtained by rotating the solution for a sphere at zero angle of attack. The old IVS was obtained by calculating a zero angle of attack blunt body solution, forming an initial value line (IVL), calculating the supersonic flow field up to the outgoing characteristic from the foot of the IVL, rotating this limiting characteristic around the free stream velocity vector, and pitching over to the correct angle of attack.

The new IVS program works in a similar manner up through the generation of the IVL. After the IVL is generated, the Rotationally Symmetric Method of Characteristics solution is carried sufficiently far around the sphere so that data along a series of lines (one line for each meridian plane) can be determined by interpolation; these lines are then rotated around the freestream vector and the resulting plane pitched over by the angle of attack. The resulting plane is now perpendicular to the body axis and situated at the sphere-body juncture (see Figure 2). In theory, the shaded region shown in Figure 2 could also be calculated by rotationally symmetric means but the resulting surface geometry is too complex to permit general use. Therefore, the constant body station IVS represents a good compromise, and is a great improvement over the previous program.

The IVS program consists of four separate programs, all connected together through an OVERLAY sequence. These programs are:

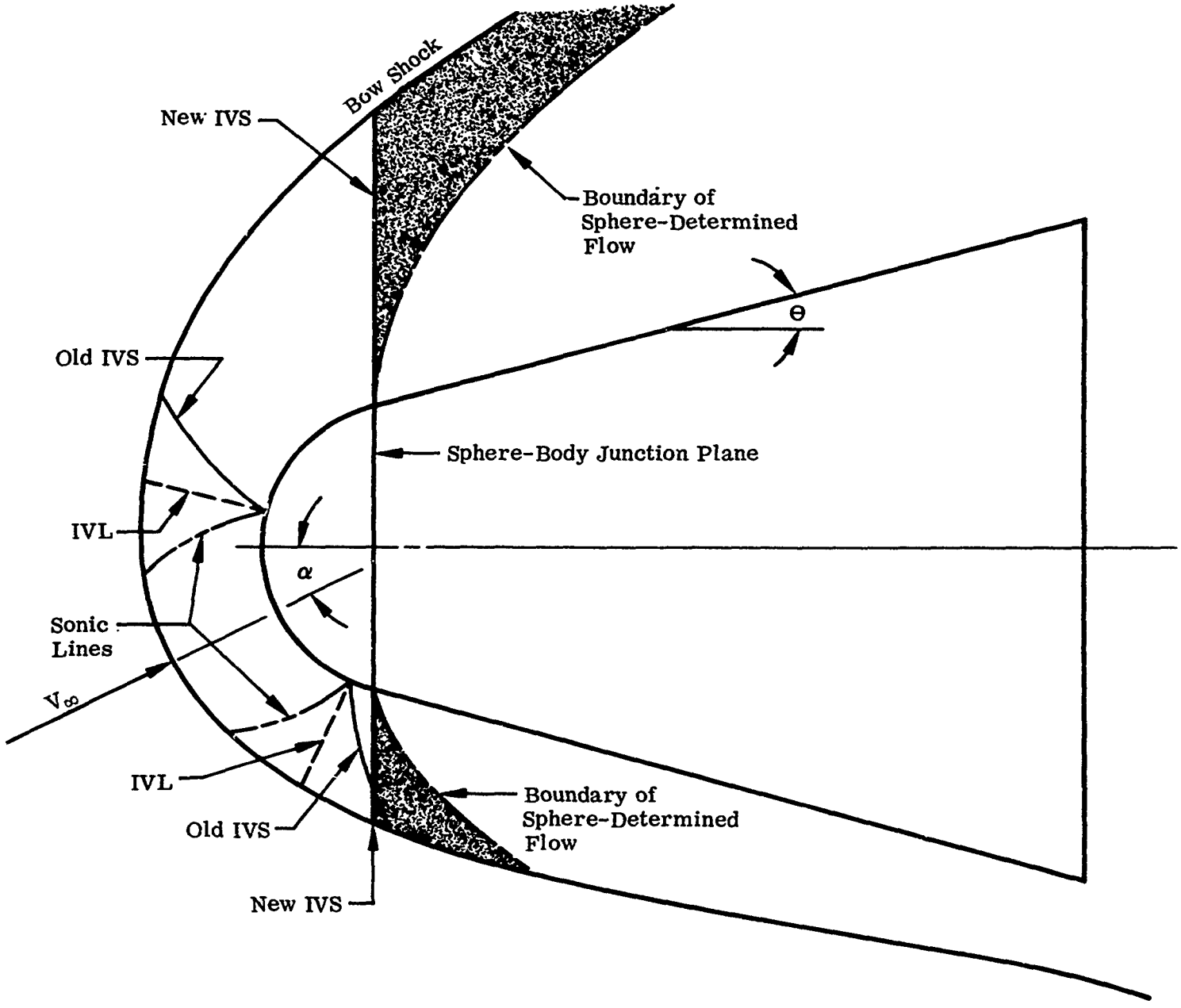

FIGURE 2. COMPARISON BETWEEN OLD AND NEW INITIAL VALUE SURFACES

(1) Blunt Body Program

(2) Initial Value Line Interpolation Program

(3) Rotationally Symmetric Method of Characteristics Program

(4) Initial Value Surface Interpolation Program

The Blunt Body Program determines the subsonic through slightly supersonic flow over the blunted nose. The Initial Value Line Interpolation Program interpolates in the Blunt Body Program data to develop a start line for the Rotationally Symmetric Method of Characteristics Program. This latter program calculates the required remaining supersonic flow field over the nose. The Initial Value Surface Interpolation Program interpolates in the RSMoC-generated data to determine properties on a plane normal to the body axis, given the number of data rings and the number of meridian planes. Each of these programs is discussed below.

1. BLUNT BODY PROGRAM

The theoretical foundations of this program were discussed in Reference 1. No significant logic changes were made to the program, and so the following discussion is essentially a summary of the approach.

The flow field behind the detached bow shock wave of the spherical nose is calculated by an extension of Van Dyke's method (Reference 2), and is an indirect one (i.e., the calculation proceeds from a specified shock to an unknown body). The shape of this unknown body is compared with that of the desired body, and appropriate changes are made in the shock wave shape until the difference between calculated and desired bodies is acceptable.

The calculation is carried out in a curvilinear orthogonal coordinate system based on the assumed shock wave. The shock wave is taken as a general conic

$$Y^2 = 2RX - BX^2 \qquad (1)$$

where X and Y are the usual Cartesian coordinates, R is the radius of curvature of the shock wave at the origin, and B is the "bluntness." The shock is hyperbolic for $B<0$, parabolic for $B=0$, and elliptic for $B>0$. By comparing Equation (1) with the standard form of the conic equation, it can be seen that for $B>0$, $B=b^2/a^2$; where b is the semi-axis in the Y direction, and a the semi-axis in the X direction. Therefore, $B=1$ corresponds to a circle or a sphere.

A curvilinear orthogonal coordinate system, ξ, η, based on the shock wave shape of Equation (1) then can be erected. The relationship between the Cartesian and curvilinear coordinates can be shown to be

$$\frac{X}{R} = \frac{1}{B}\left[1-\sqrt{(1-B\xi^2)(1-B+B\eta^2)}\right] \tag{2}$$

and

$$\frac{Y}{R} = |\xi|\eta \tag{3}$$

where the shock wave corresponds to $\eta = 1$. Figure 3 illustrates this coordinate system.

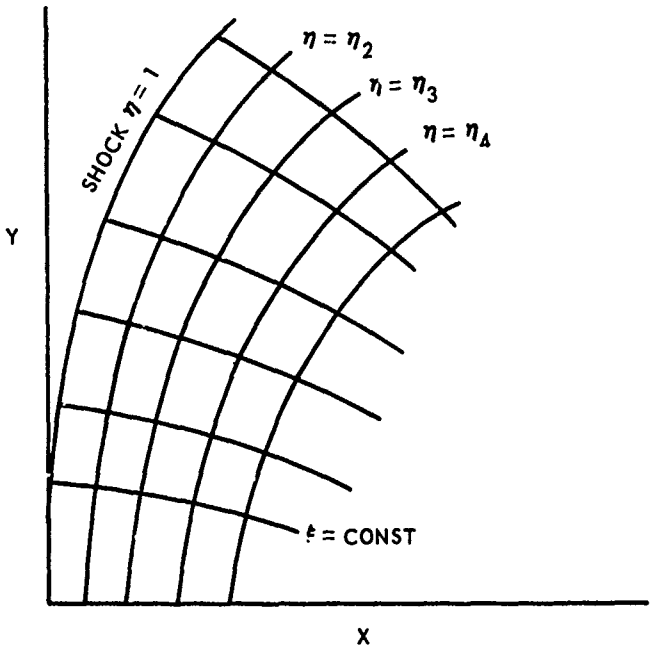

FIGURE 3. CURVILINEAR COORDINATE SYSTEM

To circumvent certain singularities in the governing gas system of dynamics equations, the first ξ used by the finite-difference solution is taken to be $\Delta\xi/2$; for succeeding values, $\xi_n = \xi_{n-1} + \Delta\xi$. Note that the body will not correspond to a constant η surface.

By introducing a Stokes' stream function, Ψ,

$$P/\rho^{\gamma} = f(\Psi) \tag{4}$$

the governing gas dynamics equations can be shown to be

$$P_\eta = \left[\rho(C\xi^2+\eta^2) + \frac{1-B\xi^2}{(\xi\eta)^{2\nu}}\,\psi_\xi^2\,\frac{\left(\frac{\partial(S/R)}{\partial P}\right)_\rho}{\rho\left(\frac{\partial(S/R)}{\partial\rho}\right)_P}\right]^{-1}\left\{\frac{1-B\xi^2}{(\xi\eta)^{2\nu}}\,\frac{(S'/R)\psi_\xi^2\psi_\eta}{\rho\left(\frac{\partial(S/R)}{\partial\rho}\right)_P} + \right.$$

$$\frac{1-B\xi^2}{(\xi\eta)^{2\nu}}\,\psi_\xi^2\left[\frac{\eta}{C\xi^2+\eta^2}+\frac{\nu}{\eta}-\frac{\psi_{\xi\eta}}{\psi_\xi}\right]+\frac{\eta}{C\xi^2+\eta^2}\,(C+B\eta^2)\,\frac{\psi_\eta^2}{(\xi\eta)^{2\nu}}-$$

$$\left.(1-B\xi^2)\,\frac{\psi_\xi\psi_\eta}{(\xi\eta)^{2\nu}}\left[\frac{B\xi}{1-B\xi^2}+\frac{\nu}{\xi}-\frac{\psi_{\xi\xi}}{\psi_\xi}+\frac{(S'/R)\psi_\xi-\left(\frac{\partial(S/R)}{\partial P}\right)_\rho P_\xi}{\rho\left(\frac{\partial(S/R)}{\partial\rho}\right)_P}\right]\right\} \qquad (5)$$

and

$$\psi_{\eta\eta} = \left\{(C+B\eta^2)\,\frac{\psi_\eta^2}{(\xi\eta)^{2\nu}}\left[-\frac{C\xi}{C\xi^2+\eta^2}-\frac{\nu}{\xi}+\frac{\psi_{\eta\xi}}{\psi_\eta}-\frac{(S'/R)\psi_\xi-\left(\frac{\partial(S/R)}{\partial P}\right)_\rho P_\xi}{\rho\left(\frac{\partial(S/R)}{\partial\rho}\right)_P}\right]-\right.$$

$$\left.\frac{C\xi}{C\xi^2+\eta^2}\,(1-B\xi^2)\,\frac{\psi_\xi^2}{(\xi\eta)^{2\nu}}+\rho(C\xi^2+\eta^2)\,P_\xi\right\}\frac{(\xi\eta)^{2\nu}}{(C+B\eta^2)\psi_\xi}+$$

$$\left[-\frac{B\eta}{C+B\eta^2}+\frac{\nu}{\eta}+\frac{(S'/R)\psi_\eta-\left(\frac{\partial(S/R)}{\partial P}\right)_\rho P_\eta}{\rho\left(\frac{\partial(S/R)}{\partial\rho}\right)_P}\right]\psi_\eta \qquad (6)$$

Note that, while P_η is a function of ψ_ξ, ψ_η, $\psi_{\xi\eta}$, $\psi_{\xi\xi}$, and P_ξ, $\psi_{\eta\eta}$ is a function of ψ_ξ, ψ_η, $\psi_{\xi\eta}$, P_ξ, and P_η. Therefore Equation (5) must be evaluated to provide P_η for Equation (6).

In Equations (5) and (6), S'/R denotes $\frac{d(S/R)}{d\psi}$ (since S is only a function of ψ in the fluid mechanics sense). For an ideal gas, the entropy derivatives reduce to:

$$\left(\frac{\partial(S/R)}{\partial \rho}\right)_P = -\frac{\gamma}{\gamma-1}\frac{1}{\rho} \tag{7}$$

$$\left(\frac{\partial(S/R)}{\partial P}\right)_\rho = \frac{1}{\gamma-1}\frac{1}{P} \tag{8}$$

and

$$\frac{d(S/R)}{d\psi} = \frac{1}{\gamma-1}\frac{f'}{f} \tag{9}$$

where $P/\rho^\gamma = f$.

The computation scheme is as follows:

1. On the shock, determine all properties at a series of evenly spaced points.
2. Determine the ξ derivatives.
3. Determine the P_η and $\psi_{\eta\eta}$ values from Equations (5) and (6).
4. Integrate into the field one $\Delta\eta$ step by using the following:

$$P_2 = P_1 - (\Delta\eta)(P_\eta)_1 \tag{10}$$

$$(\psi_\eta)_2 = (\psi_\eta)_1 - (\Delta\eta)(\psi_{\eta\eta})_1 \tag{11}$$

and

$$\psi_2 = \psi_1 - \left(\frac{\Delta\eta}{2}\right)(\psi_{\eta_1} + \psi_{\eta_2}) \tag{12}$$

5. Knowing P and ψ at the new η coordinate, evaluate all the necessary properties.
6. By numerical means, determine the ξ derivatives of P, ψ, P_η, ψ_η, and ψ_ξ at the new coordinate line.
7. Calculate P_η and $\psi_{\eta\eta}$ at the new coordinate line, using Equations (5) and (6).

8. Determine the appropriate physical properties at the new coordinate line, by an "external iteration" on the pressure through the following equation:

$$\bar{P}_2 = \bar{P}_1 - \frac{\Delta\eta}{2}(P_{\eta_1} + P_{\eta_2}) \tag{13}$$

Note that $\bar{P}$ is used only to evaluate the flow field properties at the new point, and not to reevaluate P_η or $\psi_{\eta\eta}$.

9. Thus the properties and derivatives at the new coordinate line are known, and this line then may be used as a base from which another new coordinate line can be calculated.
10. This scheme is continued until negative values of the stream function are obtained. The body location is found by extrapolating data from the last three surfaces having $\psi > 0$ to determine where $\psi = 0$.

Using the marching technique previously outlined in steps 1-10, the flow field from the shock to the body can be determined. The actual calculation of the body, however, requires special techniques. The marching technique is used until values of ψ less than zero appear. It has been found that P_η, ψ_η, and $\psi_{\eta\eta}$ all change drastically inside the body, and cannot be used to determine the body location by interpolation. Therefore, data from the last three η = constant lines are used to extrapolate to the $\psi = 0$ point to determine the body. For each η = constant line, η_{body}, P, ψ_η and $\psi_{\eta\eta}$ also are extrapolated as a function of η to η_{body}. Since the entropy at the body surface is equal to that behind a normal shock, all properties at the body surface can be determined.

Figure 4 illustrates a complete solution for $M_\infty = 8.8$ in air. Note that each $\Delta\eta$ step requires the dropping of six end points from the analysis. This is a result of using the finite-difference differentiation technique. To determine P_ξ, three points on either side must be used. Hence, the last P_ξ that can be determined is the fourth from the end of the η = constant line. After the first forward integration has occurred, P_ξ on the new line must be determined; again, the last three points are required to determine the value for the fourth from the end. Thus a total of six points must be dropped for every step taken into the flow field.

The determination of the body shape is based on the assumption that a conic shock will yield a conic body. Hence the body equation can be written as:

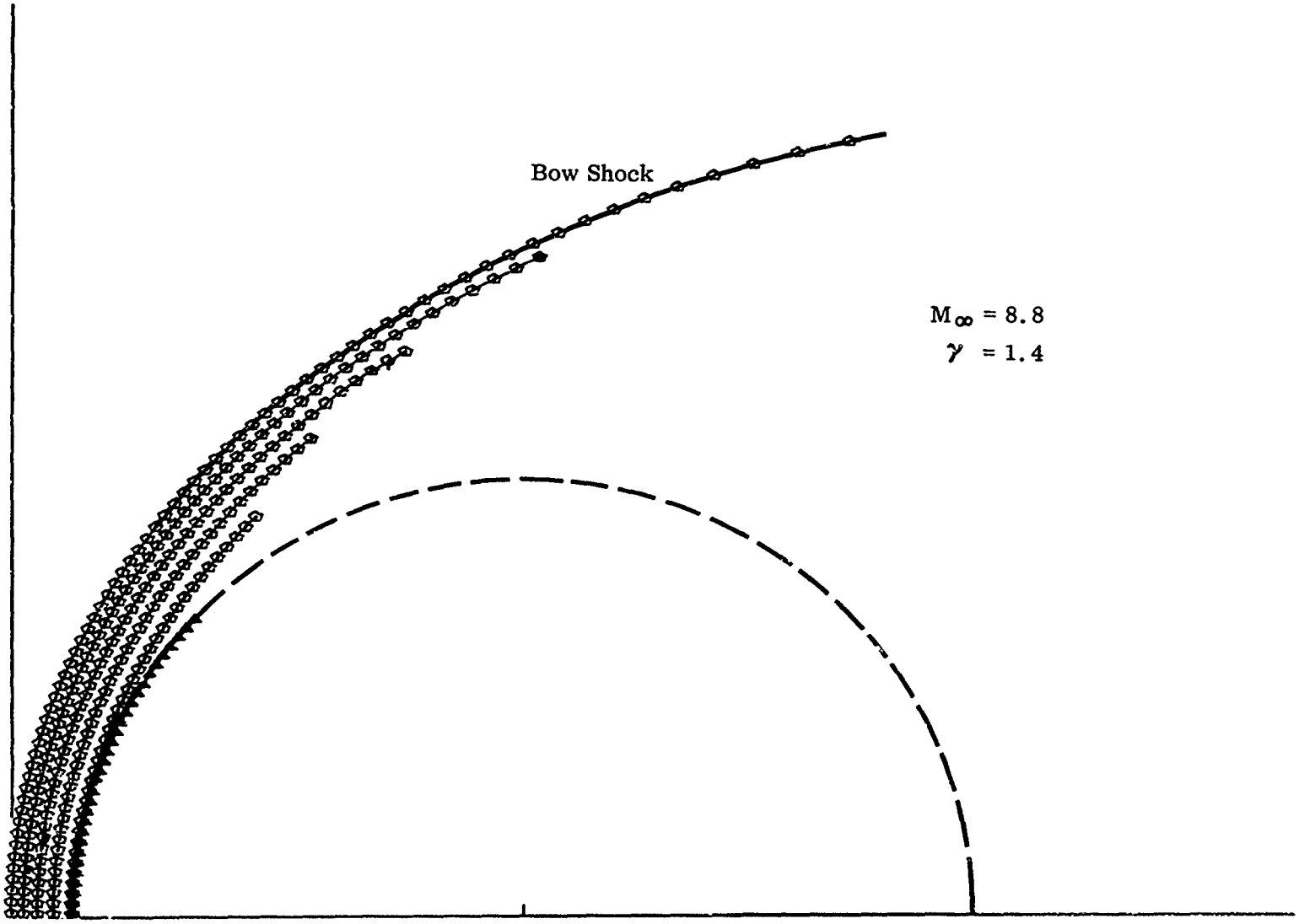

FIGURE 4. COMPLETE FLOW FIELD FOR A SPHERE

$$Y_B^2 = 2R_B(X_B-\Delta) - B_B(X_B-\Delta)^2 \qquad (14)$$

where R_B = radius of curvature of the body at the origin, referenced to R of the shock wave

B_B = body bluntness

Δ = shock stand-off distance, referenced to R of the shock wave

To determine the best values for R_B, B_B, and Δ for the N body points determined by the program, the following set of simultaneous equations (which represent the least-square solution to the body description equation with an off-set axis) must be solved for α, β, and γ:

$$\alpha N + \beta\Sigma X_i + \gamma\Sigma X_i^2 = \Sigma Y_i^2 \qquad (15)$$

$$\alpha\Sigma X_i + \beta\Sigma X_i^2 + \gamma\Sigma X_i^3 = \Sigma X_i Y_i^2 \qquad (16)$$

$$\alpha\Sigma X_i^2 + \beta\Sigma X_i^3 + \gamma\Sigma X_i^4 = \Sigma X_i^2 Y_i^2 \qquad (17)$$

where Σ denotes summation from i = 1 to N, and X_i, Y_i are the Cartesian coordinates of the body points.

The body parameters then are determined from the following functions of α, β, and γ:

$$\alpha = -\Delta(2R_B + B_B\Delta) \qquad (18)$$

$$\beta = 2(R_B + B_B\Delta) \qquad (19)$$

$$\gamma = -B_B \qquad (20)$$

The summations indicated in Equations (15), (16), and (17) include only subsonic body points. It has been found that the supersonic body points tend to deviate from a conic section rapidly, and that a more consistent body description can be obtained by excluding them. Similarly, it has been found that if the body point data are obtained from one or more $\Delta\eta$ steps, a poor body description results. This difficulty can be eliminated by providing a means for encompassing all the body points with one $\Delta\eta$ step. This is not to say that by arranging for a one-$\Delta\eta$-step body the accuracy is increased. What is obtained is a smoother, more uniform variation

of B_B with B, which permits the use of an automated iteration.

Let the $\Delta\eta$ step from the shock to the body stagnation point be $\Delta\eta_{stag}$, the $\Delta\eta$ step from the body stagnation point to the body sonic point be $\Delta\eta_B$, and the ratio of $\Delta\eta$'s for successive steps be G (a constant). Elementary series summation analysis then shows that if n is the number of steps to the body[1] the following equation can be used to determine G:

$$G - \left(1 + \frac{\Delta\eta_B}{\Delta\eta_{stag}}\right) + \left(\frac{\Delta\eta_B}{\Delta\eta_{stag}}\right) G^{-n} = 0. \tag{21}$$

Knowing $\Delta\eta_{stag}$ and $\Delta\eta_B$ and specifying n, Equation (21) may be solved by Newton's method for G. The initial value of $\Delta\eta (=\Delta\eta_o)$ is determined by:

$$\Delta\eta_o = \Delta\eta_{stag} + \frac{G-1}{G^n - 1} \tag{22}$$

In practice, $\Delta\eta_{stag}$ and $\Delta\eta_B$ are unknown initially. A first problem is calculated with G = 1.0 and $\Delta\xi = \Delta\eta = 0.02$ to determine where the body lies. Using data from this run, and extrapolating for the body sonic point if necessary, a first approximation for $\Delta\eta_{stag}$ and $\Delta\eta_B$ can be obtained. With each successive calculation, new values of the increments are calculated so as to provide the best possible fit to the body.

Certain safety factors are built into the computer program to ensure that all body points lie in the same $\Delta\eta$ step. The $\Delta\eta$ step to the stagnation point is reduced by two percent, and the distance to the sonic point increased by 30 percent. Hence:

$$\Delta\eta_{stag} = (1.0 - \eta_{stag})\ 0.98 \tag{23}$$

and

$$\Delta\eta_B = (1.0 - \Delta\eta_{stag} - \eta_{sonic})\ 1.30 \tag{24}$$

These safety factors are not optimum; they merely work.

---

[1]Note that if n is the number of steps from the shock to the body, there will be n+1 constant η lines plus the body, or n+2 series of data.

The overall iteration scheme for determining the shock wave corresponding to a given body is based on the fact that B_B is a monotonically increasing function of B, as shown in Figure 5.

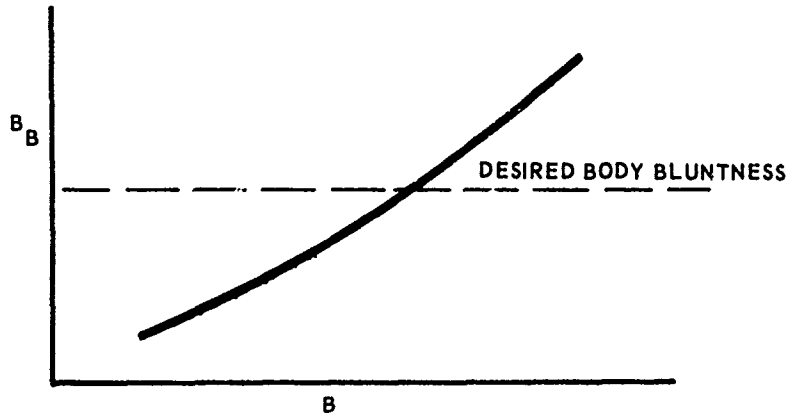

FIGURE 5. BODY BLUNTNESS AS FUNCTION OF SHOCK BLUNTNESS

The iteration process takes the first computed body bluntness and compares it with the desired bluntness. If the calculated bluntness is not sufficiently close to the desired value the shock bluntness is adjusted, for the first pass only, by the following:

$$B_2 = B_1\left(\frac{B_{B\,wanted}}{B_{B_1}}\right) \tag{25}$$

For succeeding calculations the present and past (B, B_B) pairs are retained and the new B determined by:

$$B_3 = \frac{B_2 - B_1}{B_{B_2} - B_{B_1}}\left(B_{B\,wanted} - B_{B_2}\right) + B_2 \tag{26}$$

The value of B_B, as determined by a least squares curve fit, is a weak function of the number of points used in the curve fit. During the iteration process, successive body descriptions differ in the number of body points obtained until convergence is near. As a result, there are a number of essentially parallel curves in Figure 5, one for each different number of body points. In passing from one curve to another, the quantity $(B_2 - B_1)/(B_{B_2} - B_{B_1})$, the calculated local slope, may be negative.

In this case, the iteration process governed by Equation (26) no longer provides a rational answer. When the quantity $\Delta B/\Delta B_B$ is negative, the calculation procedure then merely adds an increment to the existing value of B equivalent to that used in the last pass:

$$B_3 = B_1 + |B_1 - B_2| \tag{27}$$

This permits the iteration process to continue, and provides a chance for the natural convergence process to come into play.

As noted above, a first problem is run to determine the location of the body. The B for this run is calculated by an approximate curve fit to the data given in Reference 2.

$$B = 0.5 - 0.559\,(M_\infty - 1.0)^{-1.19} \tag{28}$$

After the first problem is run with a G = 1.0, a second is run with a calculated G but the same B. Thereafter, the iteration process discussed above takes over.

The blunt body computer program is subject to certain limitations which are described below:

1. The number of shock points is limited to 100.
2. The number of steps to the body is limited to less than 10 but more than 2.
3. A limit of 9 overall calculations is imposed on each run, due to instability of the method. For normal use, 6 is recommended.
4. For shock waves with $B>0$, $\xi^2_{max} = \left[(n-\frac{1}{2})\Delta\xi\right]^2$ must be less than $(M_\infty^2-1)/\left[(M_\infty^2-1)B+1\right]$. At this point the shock wave has degenerated into a Mach wave, and further shock angle decay is forbidden. If this occurs, the program automatically reduces the value of $\Delta\xi$ (normally equal to 0.02) to accommodate the desired number of points. In such cases it is recommended that the number of shock points be reduced to maintain $\Delta\xi \approx 0.02$.
5. In the supersonic region of the flow field, the denominator of Equation (5),

$$\left[\rho(C\xi^2+\eta^2) + \frac{1-B\xi^2}{(\xi\eta)^{2\nu}}\,\psi_\xi^2\,\frac{\left(\frac{\partial(S/R)}{\partial p}\right)_\rho}{\rho\left(\frac{\partial(S/R)}{\partial \rho}\right)_p}\right]$$

eventually goes down to zero. If this occurs within the region of calculation, the data beyond this point are meaningless and are, therefore, dropped. This will cause the program occasionally to drop more than 6 points on a given line.

2. INITIAL VALUE LINE INTERPOLATION PROGRAM

Upon completion of the flow field evaluation portion of the Blunt Body Program all of the flow field data points are available on TAPE 4 for use in determining the IVL. Using these data, this program will determine data on a straight line from the body to the shock such that the characteristic directions at every point lie on the downstream side of the IVL.

One significant change was worked into the IVL program. In the earlier program, a value of 1.05 was specified internally for M_{body}, the Mach number on the body at the foot of the IVL. This quantity is now an input variable. A value of 1.05 is recommended for all Mach numbers greater than 2.5, and a value of 1.10 for Mach numbers less than 2.5. The large M_{body} at the lower Mach numbers is due to the poor definition of the flow properties by the Blunt Body Program in the very low transonic range.

The sonic line on a rotationally symmetric blunt body takes one of two basic shapes, depending on whether the freestream Mach number is greater or less than approximately 5.0. These shapes are illustrated in Figure 6.

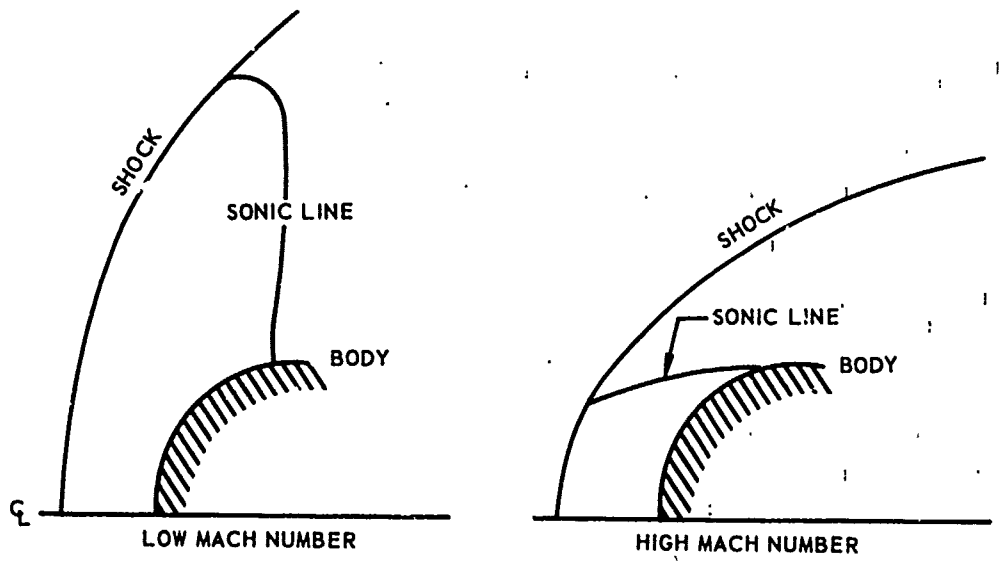

FIGURE 6. SONIC LINE SHAPES

The IVL program examines the first supersonic point on each of the "shock-like" coordinates and determines which of these will minimize the slope (which is negative) of a line between each of these points and the center of the body. The program then determines the approximate slope of the sonic line at the body by using the location of the body sonic point and the sonic point in the field nearest to the body. If this latter slope is more positive than the previously discussed slope, a high Mach number configuration exists; if the latter slope is the more negative of the two, a low Mach number configuration exists.

For the high Mach number case, the line from the center of the body passing through the point on the body where $M = M_{body}$ is chosen as the IVL; the data interpolation takes place along this line.

For the low Mach number case, the sonic line is highly curved and is actually made up of the outer portion of the right-running limiting characteristic and the inner portion of the left-running limiting characteristic. In this situation, if the high Mach number method of determining the IVL were to be used, the IVL would pass through the subsonic region. Thus, a data line with a different slope and a different intercept point on the body is needed. This slope is obtained by taking the slope of the innermost segment of the sonic line (the calculation of which has been discussed above) and rotating it five degrees clockwise.

A table of body point coordinates and associated left-running characteristic angles, $\delta + \mu$ (where δ is the local flow angle and μ the Mach angle), is prepared to go from the body point data and an interpolation performed to determine the location of the body point whose left-running characteristic direction corresponds to the IVL slope. Having thus defined a point on the IVL and its slope, the interpolation for the data points throughout the flow field can be carried out. However, the body point determined by this method is not used as a point on the IVL. Due to the drastic increase in error in calculating the local flow angles near the body for low Mach numbers, it has been found that better downstream calculations are obtained if the solution goes directly from the first field point to the body, thus ignoring the IVL body point.

As a final step, the freestream quantities, the body geometric quantities (R_B, B_B, Δ), the location and flow properties of each point on the IVL, and the mass-entropy table are printed and stored on tape for the Rotationally Symmetric Method of Characteristics Program.

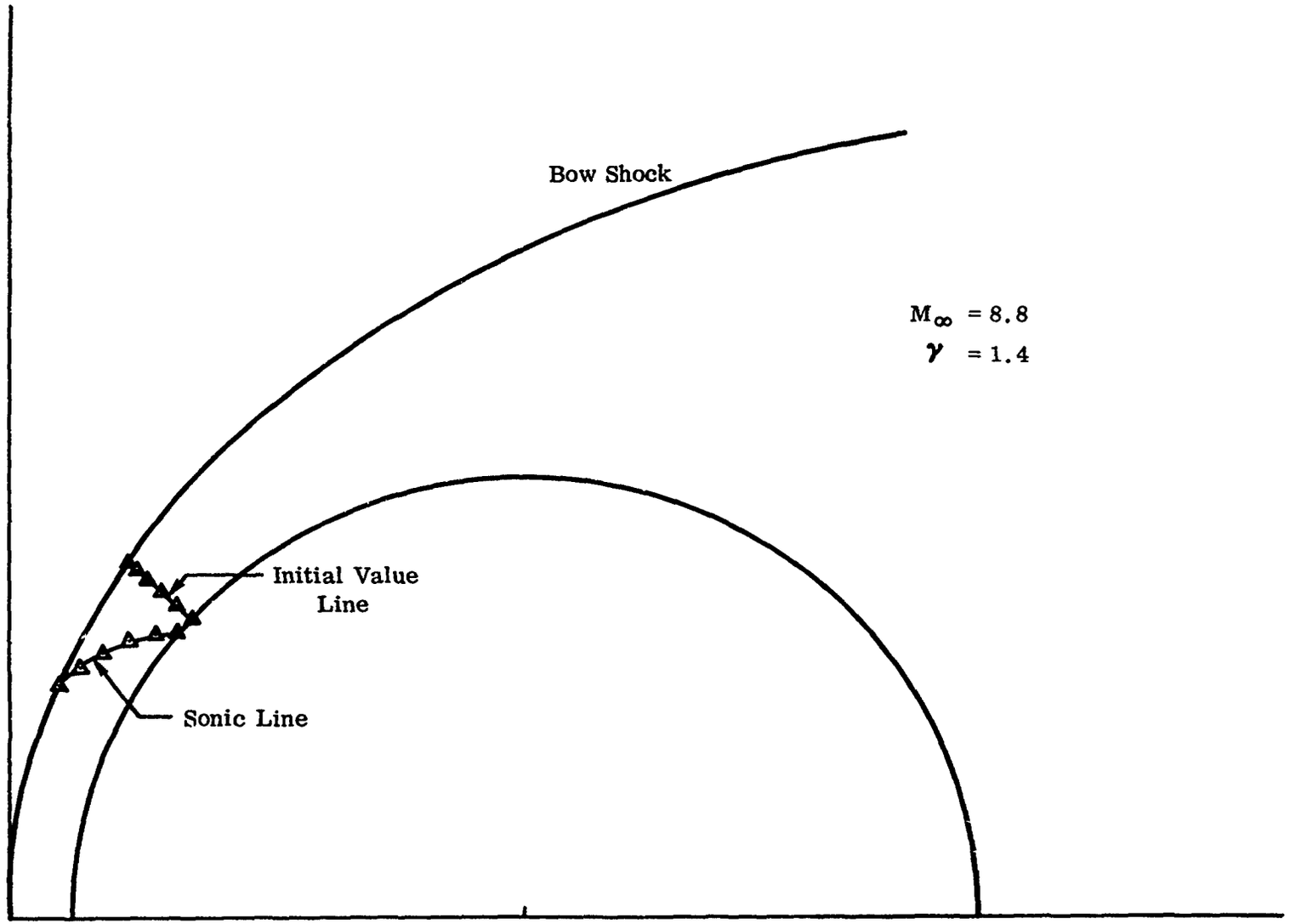

FIGURE 7. SPHERE SONIC LINE AND INITIAL VALUE LINE

The mass-entropy table is a listing of shock ordinate values and the associated total pressure ratio (or downstream entropy), starting at the stagnation line and including as the last point the shock point of the IVL. This table is used with a characteristics program to ensure an exact determination of the local total pressure (or entropy) in rotational method of characteristics procedures (Reference 3).

Figure 7 shows the body location and shape, and the interpolated sonic line and initial value line for the sphere solution shown earlier in Figure 4. In the final output, after convergence, all the blunt body data are normalized by R_{body}; therefore the body radius is here found to be 1.0.

3. ROTATIONALLY SYMMETRIC METHOD OF CHARACTERISTICS PROGRAM

Using the initial value line as starting data the Rotationally Symmetric Method of Characteristics (RSMoC) program calculates the supersonic flow over the sphere-cone body. These supersonic calculations are carried out along characteristics starting at the shock wave and traveling in toward the body as well as downstream. The calculation continues until there are at least two data points on each characteristic downstream of the limit line, and one shock point is downstream of the limit line. The limit line is a line whose slope is tan ($\pi - \alpha$) and which passes a distance of $(1-\sin\Phi)$ upstream of the center of the sphere (see following section on the IVS).

The present RSMoC program represents a considerable modification of the previous RSMoC program described in Reference 1. Some of the major changes are:

(1) A mesh control scheme has been added to permit the calculation of characteristics emanating from shock points and to control the step size achieved on the body.
(2) A shock point routine using shock segments as prescribed by the mesh control program.
(3) Inclusion of the limit line to terminate the construction of characteristics.
(4) A body point routine.

The basic numerical methods are discussed below:

a. Field Point

The field point solution in the rotationally symmetric method of characteristics procedure determines the properties at the intersection of two characteristics of opposite families, using the mass-entropy method (Reference 3). A schematic of two characteristics is shown in Figure 8.

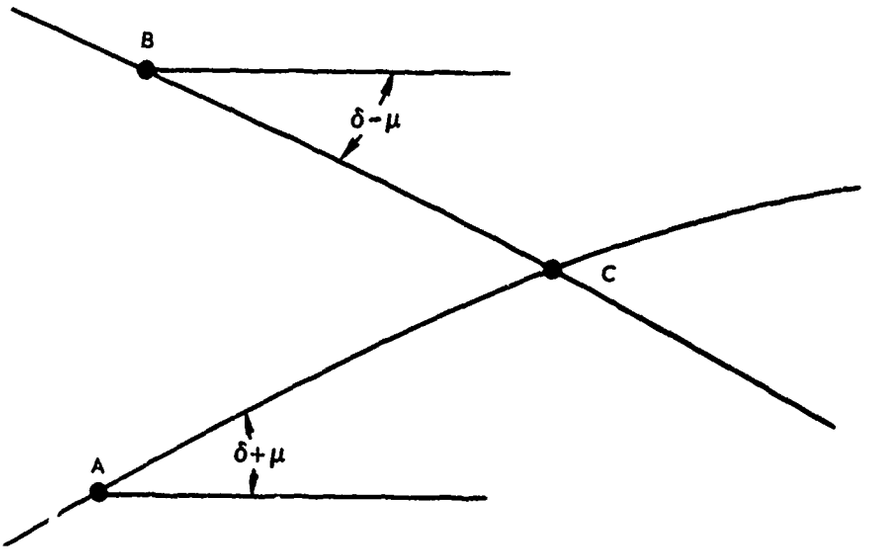

FIGURE 8. FIELD POINT CALCULATION

Points A and B in Figure 8 are known points in the flow field, and point C is to be determined. The characteristics connecting the "base points" (points A and B) with the unknown field point are approximated by straight lines having a slope determined by averaging the characteristic direction at the known base point with the best available value at the unknown field point. To start the process, the properties at C are assumed to be an average of those at A and B. Let point B be the point situated on the right-running characteristic which lies in the $\delta-\mu$ direction (δ is the local flow direction and μ is the local Mach angle), and let A be the point on the left-running characteristic which lies in the $\delta+\mu$ direction.

The characteristic passing through B can be approximated by

$$\frac{Y_C - Y_B}{X_C - X_B} = \tan\left(\overline{\delta-\mu}^{BC}\right) \equiv T_B \qquad (29)$$

where

$$\left(\overline{\delta-\mu}^{BC}\right) \equiv \frac{1}{2}\left(\delta_B-\mu_B+\delta_C-\mu_C\right)$$

and the characteristic passing through A can be approximated by

$$\frac{Y_C-Y_A}{X_C-X_A} = \tan\left(\overline{\delta+\mu}^{AC}\right) \equiv T_A \qquad (30)$$

The intersection then is defined by eliminating Y_C from Equations (29) and (30):

$$X_C = \frac{Y_A-Y_B-(X_AT_A-X_BT_B)}{T_B-T_A} \qquad (31)$$

Equation (31), however, cannot provide accurate answers when either T_A or T_B, or both, become very large. In these cases, Equations (29) and (30) can be rewritten to use the cotangent function instead of the large values of the tangent, and the equivalent of Equation (31) can be derived.

The compatibility equation (Reference 4) can be written as:

$$\frac{d\ln P}{\gamma} - \frac{d\delta}{\sin\mu\cos\mu} + \frac{\sin\delta}{\cos\mu}\frac{dL_1}{Y} = 0 \qquad \text{on } \delta-\mu \qquad (32)$$

and

$$\frac{d\ln P}{\gamma} + \frac{d\delta}{\sin\mu\cos\mu} + \frac{\sin\delta}{\cos\mu}\frac{dL_2}{Y} = 0 \qquad \text{on } \delta+\mu \qquad (33)$$

where dL_1 is a distance along the $(\delta-\mu)$ characteristic and dL_2 is a distance along the $(\delta+\mu)$ characteristic. Equations (32) and (33) can then be written in finite-difference form as:

$$\frac{\ln(P_C/P_B)}{\gamma} - \frac{\delta_C-\delta_B}{\sin\overline{\mu}^{BC}\cos\overline{\mu}^{BC}} + \frac{\sin\overline{\delta}^{BC}}{\cos\overline{\mu}^{BC}}\frac{\Delta L_{BC}}{\overline{Y}^{BC}} = 0 \qquad (34)$$

and

$$\frac{\ln(P_C/P_A)}{\gamma} + \frac{\delta_C-\delta_A}{\sin\overline{\mu}^{AC}\cos\overline{\mu}^{AC}} + \frac{\sin\overline{\delta}^{AC}}{\cos\overline{\mu}^{AC}}\frac{\Delta L_{AC}}{\overline{Y}^{AC}} = 0 \qquad (35)$$

where $\Delta L_{BC} = \sqrt{(X_B - X_C)^2 + (Y_B - Y_C)^2}$

$\Delta L_{AC} = \sqrt{(X_A - X_C)^2 + (Y_A - Y_C)^2}$

Solving Equations (34) and (35) for δ_C,

$$\delta_C = \frac{1}{2}\left\{\ln P_A - \ln P_B + 2\gamma\left[\frac{\delta_B}{\sin 2\bar{\mu}^{BC}} + \frac{\delta_A}{\sin 2\bar{\mu}^{AC}}\right] + \gamma\left[\frac{\sin\bar{\delta}^{BC}\Delta L_{BC}}{\cos\bar{\mu}^{BC}\bar{\gamma}^{BC}} - \frac{\sin\bar{\delta}^{AC}\Delta L_{AC}}{\cos\bar{\mu}^{AC}\bar{\gamma}^{AC}}\right]\right\} \Big/ \left[\frac{\gamma}{\sin 2\bar{\mu}^{BC}} + \frac{\gamma}{\sin 2\bar{\mu}^{AC}}\right] \tag{36}$$

Similarly, solving for $\ln P_C$,

$$\ln P_C = \left\{\frac{1}{\gamma}\left[\sin 2\bar{\mu}^{BC}\ln P_B + \sin 2\bar{\mu}^{BC}\ln P_A\right] + \delta_A - \delta_B - \left[\frac{\sin\bar{\delta}^{BC}\sin\bar{\mu}^{BC}\Delta L_{BC}}{\bar{\gamma}^{BC}} + \frac{\sin\bar{\delta}^{AC}\sin\bar{\mu}^{AC}\Delta L_{AC}}{\bar{\gamma}^{AC}}\right]\right\} \Big/ \left\{\frac{1}{2\gamma}\left[\sin 2\bar{\mu}^{BC} + \sin 2\bar{\mu}^{AC}\right]\right\} \tag{37}$$

The actual computation sequence is as follows:

1. The properties at point C are set equal to averages of those at points A and B.
2. The intersection of the approximations to the characteristics is obtained from Equation (31) or its equivalent.
3. δ_C is obtained from Equation (36).
4. Both sides of Equation (37) are evaluated, and the difference between left and right sides is taken as a residual. If the absolute value of this residual is less than a prescribed amount, the solution is acceptable. Otherwise the iteration is continued.
5. If the solution is not acceptable, the new value of P_C is obtained from Equation (37).

The program retains corresponding values of P_C and its associated residual for the most recent positive and negative residual; a linear interpolation is carried out for the value of P_C corresponding to a zero residual. This process has been found to speed up the convergence process.

b. Shock Point

The calculation of the extension to the bow shock wave uses the shock point and the interpolated field point on the previously calculated characteristic, as shown in Figure 9.

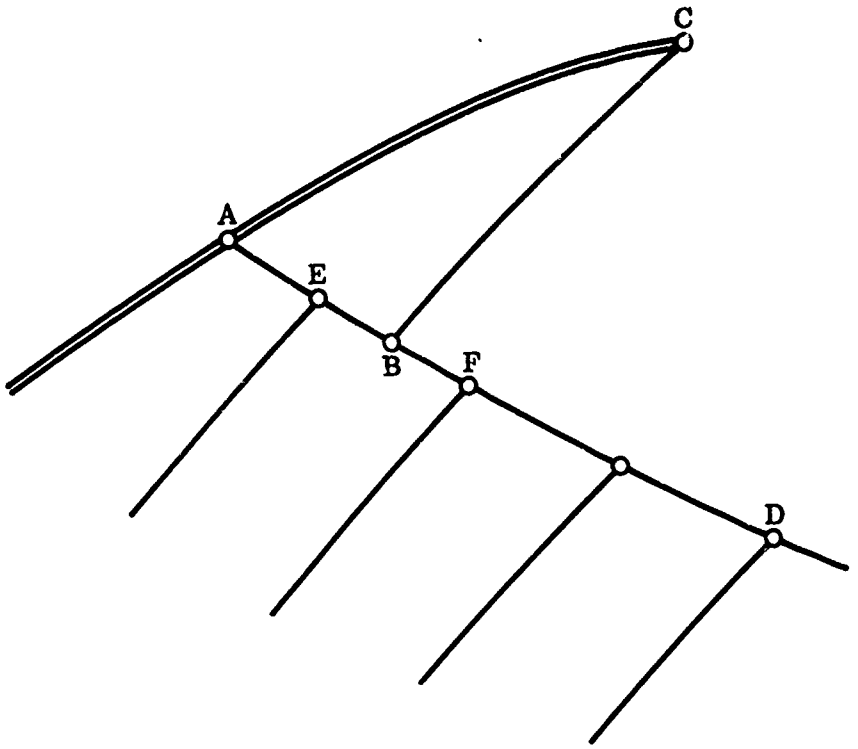

FIGURE 9. SHOCK POINT CALCULATION

The equation of the shock wave is approximated locally by:

$$\frac{Y_C - Y_A}{X_C - X_A} = \tan\left(\frac{\theta_A + \theta_C}{2}\right) = \tan(\bar{\theta}) \qquad (38)$$

The properties at point C are evaluated using the local slope of the shock wave, $\tan \theta_C$. The point B along the characteristic A-D is determined by the intersection

of the $\delta - \mu$ characteristic passing through point A and the $\delta + \mu$ characteristic passing through point C. This process is identical to the field point solution discussed previously except that the properties at B are determined by interpolation using points E and F. Thus the process is iterative in nature. Once the properties at B are determined, the compatibility equation, Equation (35), is evaluated along B-C and the residual determined. Another shock angle, θ_C, is chosen and the process repeated. Given the two residuals and the two shock wave angles, an interpolation can easily be set up to determine the shock angle for a zero residual. Using this shock angle, the corresponding residual is calculated and these shock angles and residuals are used to generate yet another shock angle. This process continues until the residual is less than 1×10^{-6}.

Since such iterative calculations are usually oscillatory and the first few oscillations may be quite wild, the first shock angle used is the shock angle that generates sonic flow behind the shock. The second approximation is taken to be the previous shock angle θ_A. These two values suffice to start the iteration.

c. Body Point

The body point solution must satisfy both a geometrical equation and the compatibility equation. As shown in Figure 10, let point A be a field or shock point and point C be the associated body point.

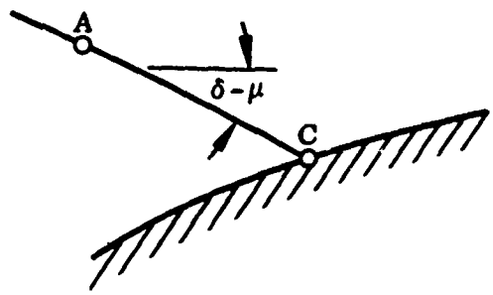

FIGURE 10. BODY POINT CALCULATION

The line connecting A and C is described by

$$Y - Y_A = m(X - X_A) \tag{39}$$

For a blunt general conic nose, located as shown in Figure 11, the equation is:

$$Y^2 = 2R(X+\Delta) - B(X+\Delta)^2 \tag{40}$$

where Δ is the displacement of the nose, positive when the displacement is to the left of the origin.

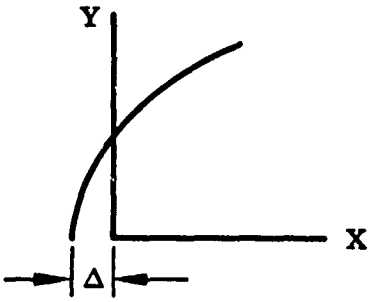

FIGURE 11. BLUNT BODY GEOMETRY

Combining Equations (39) and (40) shows that:

$$X_C = -\frac{BB}{2AA} \pm \sqrt{\left(\frac{BB}{2AA}\right)^2 - \frac{CC}{AA}} \tag{41}$$

where

$$AA = B + m$$

$$BB = 2\left[m(Y_A - mX_A) - R + B\Delta\right]$$

$$CC = (Y_A - mX_A)^2 + \Delta(B\Delta - 2R)$$

For the case of a body segment described by a general cubic equation

$$Y = C_1(X-X_0)^3 + C_2(X-X_0)^2 + C_3(X-X_0) + C_4 \tag{42}$$

an iterative solution is obtained by using the standard Newtonian method:

$$X_C^{(i)} = X_C^{(i-1)} - \frac{Y_C^{(i-1)} - (X_C^{(i-1)} - X_A)m - Y_A}{(dY/dX)_C - m} \tag{43}$$

Starting with an approximate value of X_C, values of Y_C and $(dY/dX)_C$ are determined, and used in Equation (43) to obtain a better value of X_C. This process continues until no further significant change occurs in the value of X_C.

The compatibility equation applied between A and C is

$$\frac{\gamma}{\sin 2\bar{\mu}} \left(\delta_C - \delta_A - \sin\bar{\delta} \sin\bar{\mu} \frac{\Delta L_{AC}}{\bar{\gamma}} \right) - \ln \frac{P_C}{P_A} = 0 \qquad (44)$$

For the first approximation, the residual of Equation (44) is evaluated as written and then Equation (44) is solved for P_C. This new value for P_C now determines a new residual. By interpolating, always using the two latest new values for P_C and the associated residuals, a satisfactorily small residual can be easily determined in an iteration loop.

d. Mesh Control

The method of characteristics program calculates along right running characteristics, i.e., those that originate at the shock wave and propagate downstream toward the body. The X distance between successive intersections of these characteristics and the body surface is defined as the step size of the solution. The step size is then a function of the length of shock increment used to generate new characteristics. Subroutine MESH both tests the step size to ascertain its correctness and adjusts the shock wave step size so that the desired body increment is obtained. Upon completion of a characteristic, MESH is used to accept or reject the characteristic, depending on whether the size criterion is satisfied or not. By adjusting the step size, MESH also makes certain that there is a characteristic that terminates at the sphere-cone juncture.

This characteristics program has two distinct modes of operation in determining the step size: normal operation and juncture point operation. The program switches automatically from one mode to the other, as required. The specified body step size is given the name XSTARB. For both the normal and juncture point operation modes, MESH first calculates the step size, using the body point just determined, and the body point on the previously accepted characteristic. This candidate step size is stored as DXSTAR, as shown in Figure 12.

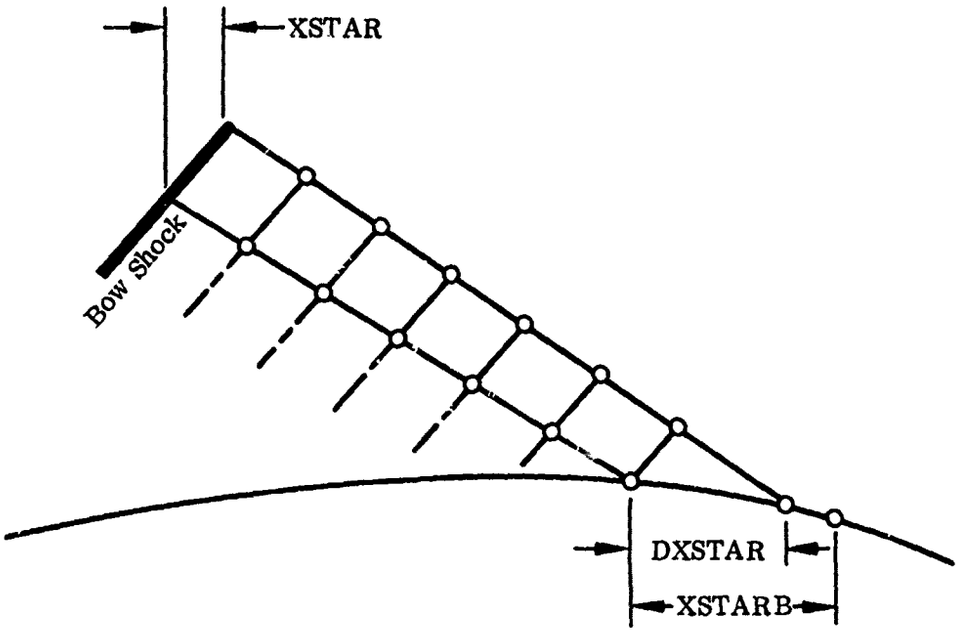

FIGURE 12. SHOCK AND BODY STEP SIZES

For positive values of DXSTAR, the program checks to see if DXSTAR is more than half but less than the full value of XSTARB. If DXSTAR satisfies these criteria, the complete characteristic is acceptable. This is the normal operation. For juncture point operation, the program checks to see whether the distance between the last body point and the juncture point is greater than 1.2(XSTARB). If the distance is greater, the program returns control to the main program, after adjusting the shock segment length to provide a step size of 0.7(XSTARB). If the distance is not greater than 1.2(XSTARB), the juncture point operation will occur for the next characteristic. Initially, the shock wave segment length is adjusted by multiplying present shock segment length by the ratio of the desired body step size to that achieved using present shock segment length:

$$\Delta S_{\text{shock}_{\text{new}}} = \Delta S_{\text{shock}_{\text{last}}} \left[\frac{\Delta X_{\text{body}_{\text{juncture point}}}}{\Delta X_{\text{body}_{\text{last}}}} \right] \qquad (45)$$

On the successive iterative passes through MESH, which occur upon the completion of a new complete characteristic, a linear interpolation is performed to determine the shock wave step size required to place the body point on the juncture point:

$$\Delta S_{\text{shock}_{i+1}} = \Delta S_{\text{shock}_o} + \left[\frac{\Delta S_{\text{shock}_i} - \Delta S_{\text{shock}_o}}{\Delta X_{\text{body}_i} - \Delta X_{\text{body}_o}}\right] \left(X_{\text{body}_{\text{jnct pt}}} - X_{\text{body}_o} \right) \tag{46}$$

When the program starts calculations from an initial value line (IVL), the IVL itself sets its own mesh size. There is no connection between mesh size in the IVL region and that requested by the user for the segment of the body downstream of the IVL. After the IVL has been used to generate a complete characteristic, the final step size in the IVL region is compared with that requested for the appropriate body segment. If the requested step size is larger than that generated in the IVL region, the rate of growth of the body step size is limited to a factor of 2.0.

e. Sample Results

Figure 13 shows a rotationally symmetric method of characteristics calculation carried downstream from the IVL given in Figure 7. Each point on the IVL generates a characteristic which moves inwards and downstream until it terminates on the body. After completing the IVL-spawned characteristics, the mesh control option is brought into play. Under this option the bow shock wave is extended and a characteristic generated to provide the desired step size along the body.

These calculations are carried downstream until two points on a characteristic lie beyond the limit line, which is the sphere-body juncture rotated clockwise about the center of the sphere by an angle equal to the angle of attack.

After passing this limit line, another mode of operation comes into play. This mode takes the final shock wave increment used to calculate a characteristic terminating on the body, and increases it by 10% for each subsequent characteristic. Each of these characteristics now terminates with a field point when two field points lie downstream of the limit line. This mode continues until a shock point is calculated which lies downstream of the limit line. This process can be traced in Figure 13.

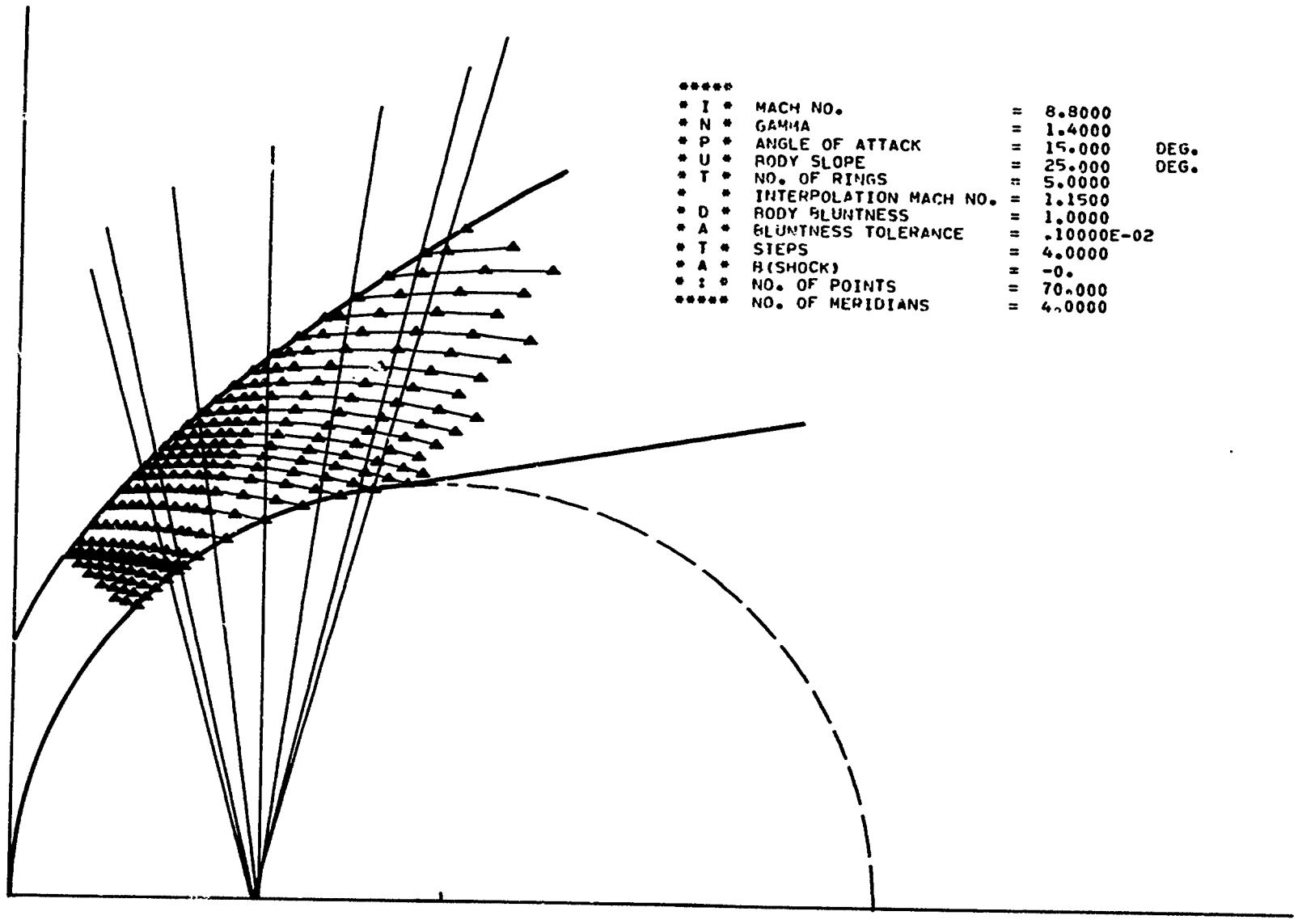

FIGURE 13. INITIAL VALUE SURFACE FLOW FIELD

4. INITIAL VALUE SURFACE INTERPOLATION PROGRAM

Having calculated the complete flow field about the spherically capped cone in a wind-axis system an interpolation is carried out along specific lines to determine the properties in each meridian plane in a body-axis system. Each line represents the sphere-body juncture rotated clockwise about the center of the sphere by an angle β which is a function of the desired meridian angle and the angle of attack. When these interpolation lines are rotated about the wind axis, they will form a plane normal to the body axis.

Figure 14 shows the constant body station plane oriented by a wind-axis system at an angle of attack, α. A meridian plane is located by the angle ψ in the wind-axis system. From the geometry it can be shown that:

$$\cos\beta = \frac{1}{\sqrt{1 + \sin^2\psi \tan^2\alpha}} \tag{47}$$

$$\sin\beta = -\sin\psi \tan\alpha \cos\beta \tag{48}$$

where β will vary between the limits of $\pm\alpha$. Note that the angle β is measured away from the vertical axis in the wind-axis system.

In Figure 13, the interpolation lines are shown for seven meridian planes. The flow properties are determined by linear interpolation at the intersection of each line and each characteristic. From Figure 13 it is seen that different lines end up with different number of interpolated points. Using these interpolated data, a second interpolation is carried out to provide the same number of points on each line, the number being the number of rings specified by the user. The geometry of the resulting surface for the case shown in Figure 13 is shown in Figure 15, where the number of rings specified was five. This initial value surface can be used for a blunted cone of 25° half-angle or a slab delta wing with 65° sweep, at a Mach number of 8.8 and an angle of attack of 15°. Figure 16 shows another solution, this time for a blunted cone at Mach 14.9 in helium at 20° angle of attack. The interpolation lines for 11 meridian planes are shown in this figure, and the resulting geometry is shown in Figure 17.

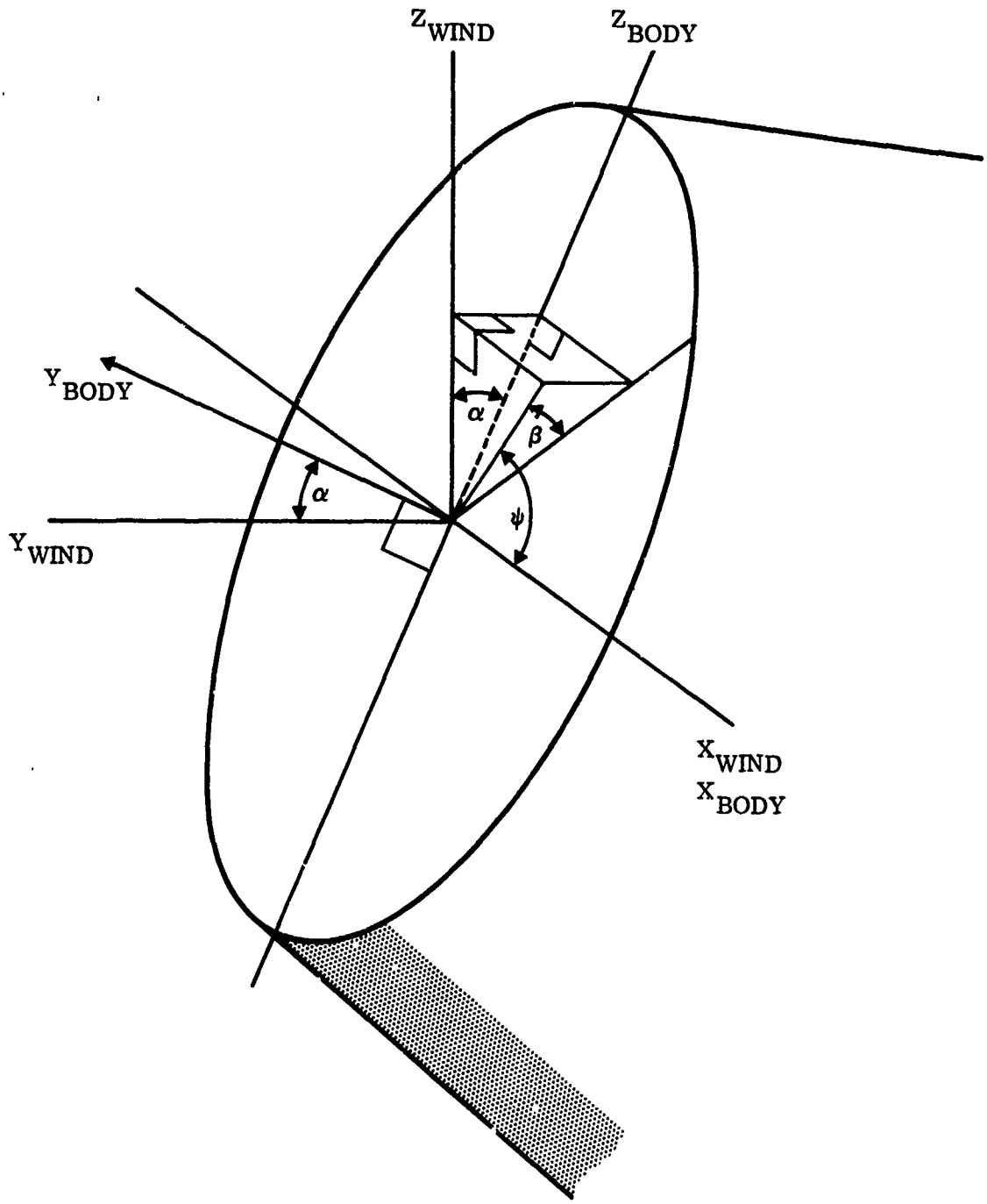

FIGURE 14. INITIAL VALUE SURFACE GEOMETRY

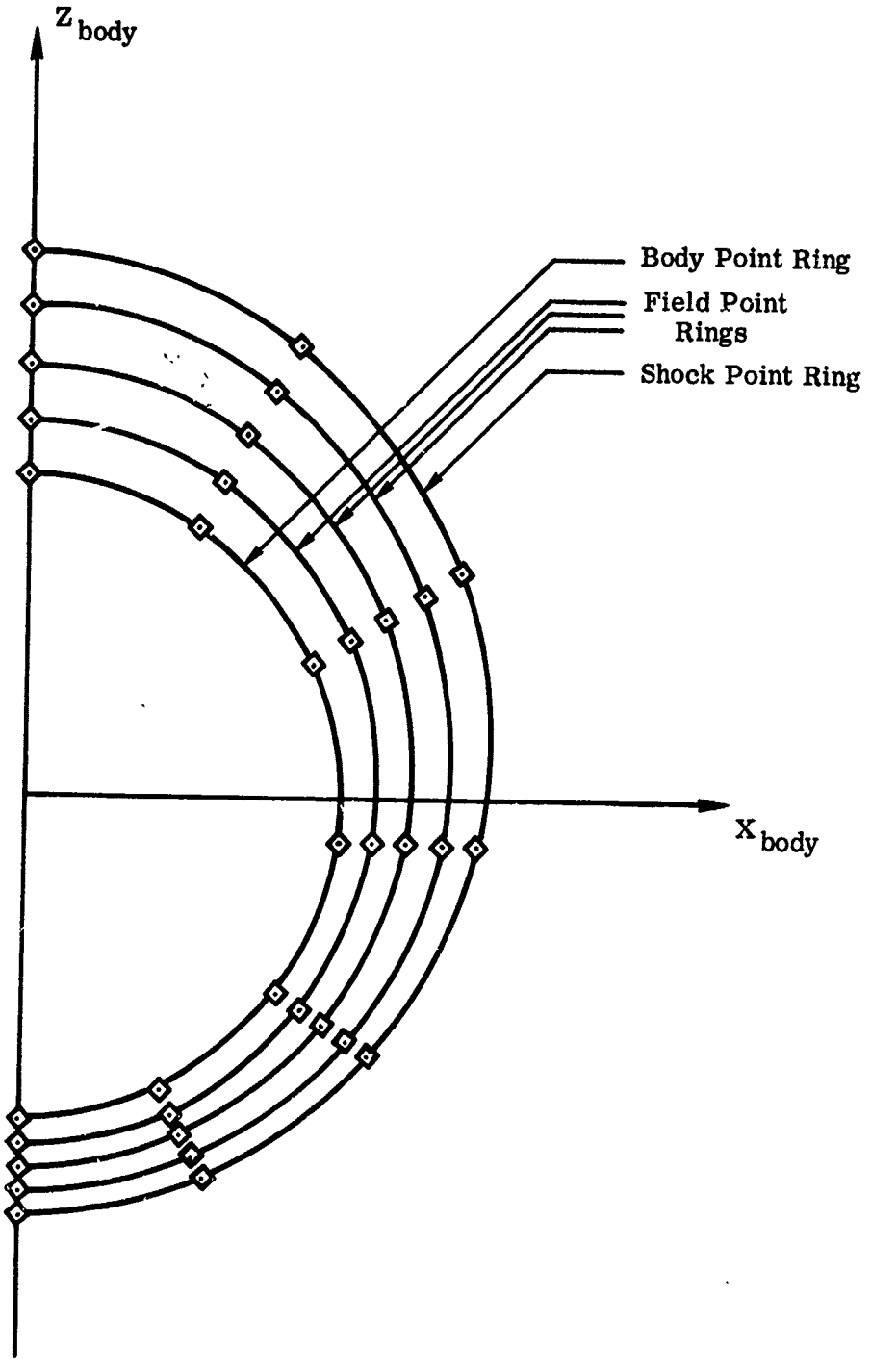

FIGURE 15. INITIAL VALUE SURFACE

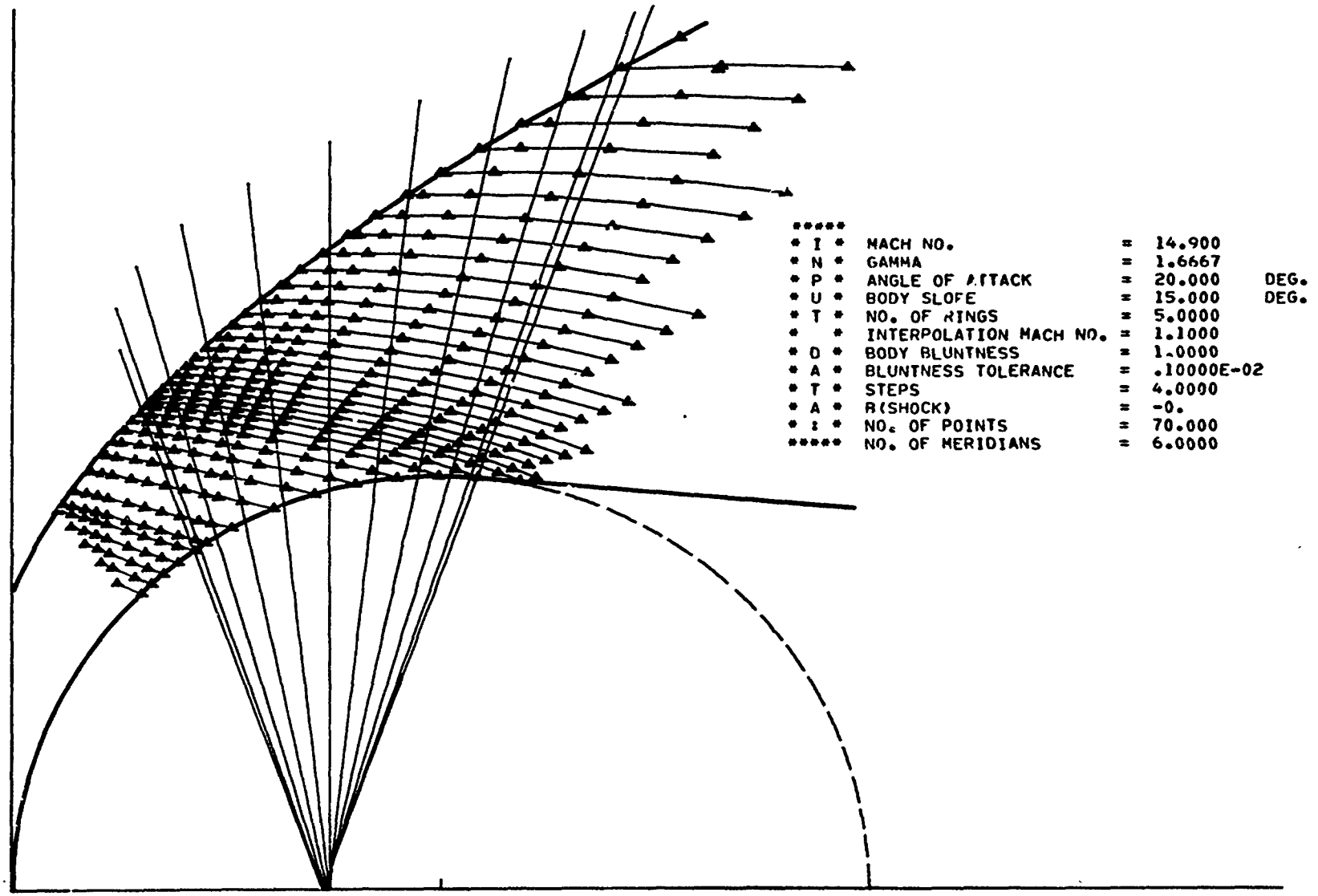

FIGURE 16. INITIAL VALUE SURFACE FLOW FIELD FOR A BLUNTED CONE AT $\alpha = 20^{o}$

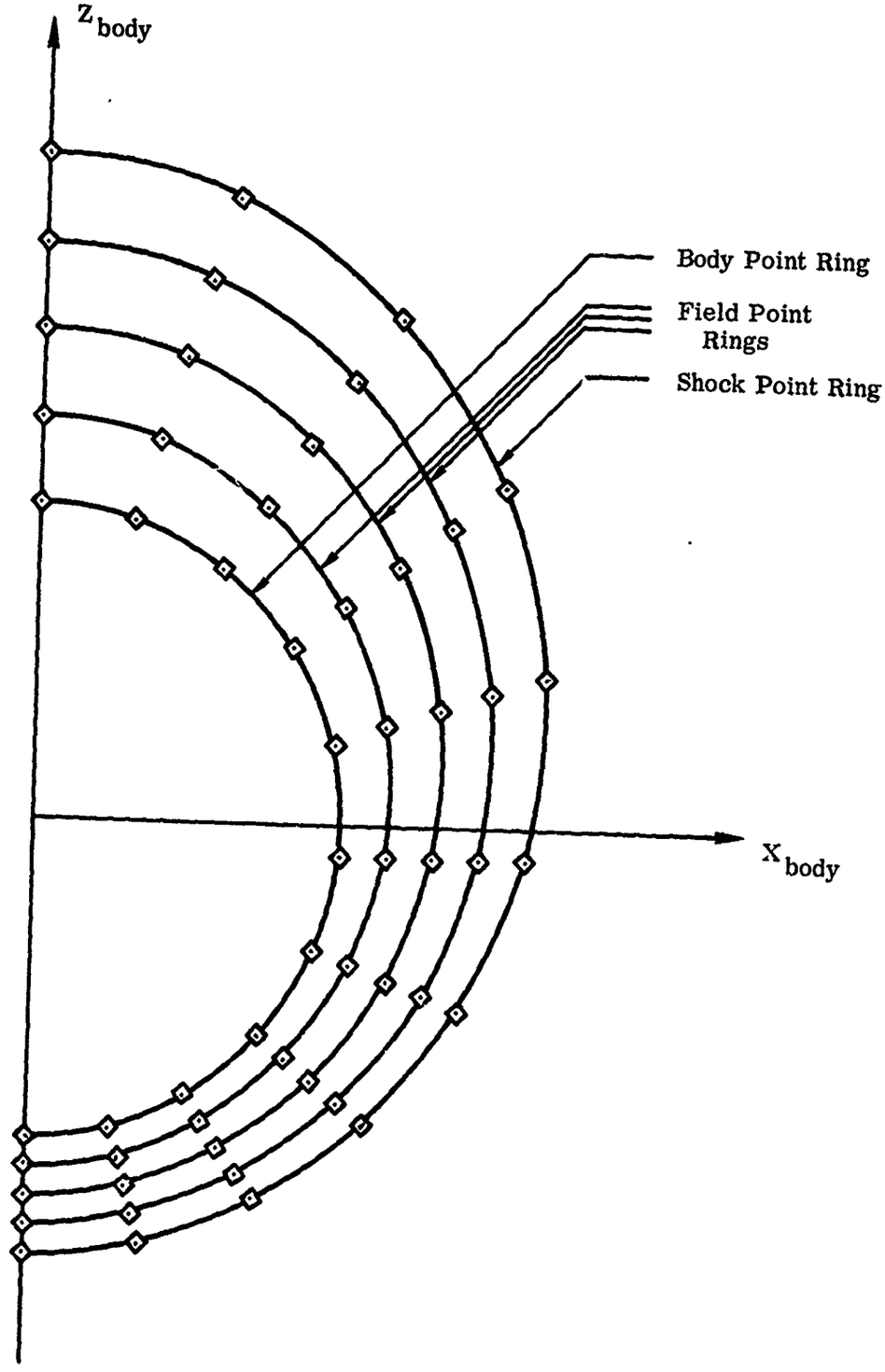

FIGURE 17. INITIAL VALUE SURFACE FOR BLUNTED CONE

SECTION IV

THE THREE-DIMENSIONAL METHOD OF CHARACTERISTICS

The original three-dimensional method of characteristics has been revised extensively. Many new approaches and procedures were used and included (Refs 5, 6). An up-to-date description of the method and computer program is presented here.

1. EQUATIONS AND ANALYSIS

The general compatibility relation for three-dimensional steady flow of a real gas in equilibrium is derived from the fundamental flow equations. In terms of pressure and flow direction angles, this relation applies to both isoenergetic and nonisoenergetic flow.

a. Fundamental Equations

The equations for steady inviscid flow are

$$\rho \nabla \cdot \vec{q} + \vec{q} \cdot \nabla \rho = 0 \tag{49}$$

$$\rho \vec{q} \cdot \nabla \vec{q} + \nabla P = 0 \tag{50}$$

$$\vec{q} \cdot \nabla s = 0 \tag{51}$$

where $\vec{q}$ is the velocity, ρ the density, P the pressure and s the specific entropy.

The gas-dynamic equation,

$$\vec{q} \cdot \nabla (q^2/2) - a^2 \nabla \cdot \vec{q} = 0 \tag{52}$$

where a is the speed of sound, is not restricted to isoenergetic flow; however, since it is sometimes derived for a uniform freestream (isoenergetic flow) only, a general derivation is given below.

Consider $P = P(\rho, s)$; since $\nabla P = (\partial P/\partial \rho)_s \nabla \rho + (\partial P/\partial s)_\rho \nabla s$ we have

$$\vec{q}\cdot\nabla P - a^2\vec{q}\cdot\nabla\rho = 0 \tag{53}$$

where

$$a^2 = (\partial P/\partial\rho)_s$$

by virtue of Equation (51). Substitution of Equations (49) and (50), and the identity

$$\vec{q}\cdot\nabla\vec{q} = (\nabla\times\vec{q})\times\vec{q} + \nabla(q^2/2)$$

into Equation (53) leads to the gas-dynamic equation (52). In rectangular coordinates Equations (52) and (50) are

$$\left.\begin{aligned} &(u^2-a^2)u_x + (v^2-a^2)v_y + (w^2-a^2)w_z + \\ &\quad uv(v_x+u_y) + vw(w_y+v_x) + wu(u_z+w_x) = 0 \\ &uu_x + vu_y + wu_z + P_x/\rho = 0 \\ &uv_x + vv_y + wv_z + P_y/\rho = 0 \\ &uw_x + vw_y + ww_z + P_z/\rho = 0 \end{aligned}\right\} \tag{54}$$

where subscripts x, y, z denote partial differentiation.

b. Derivation of Compatibility Relations

A characteristic surface allows possible discontinuities of the first derivatives of flow variables in the direction of its normals. Given initial data on such a surface, the normal derivatives of flow variables are not uniquely determined by Equation (54). Applying the methods of Reference 7 by setting the x and y axes tangent to a characteristic surface at the origin and solving for w_z in terms of u, v, w, P, and their derivatives with respect to x and y, we obtain $w_z = \det[N]/\det[D]$ where

$$\det[N] = \begin{vmatrix} u & v & (a^2-u^2)u_x + (a^2-v^2)v_y - uv(v_x+u_y) - w(uw_x+vw_y) \\ 1 & 0 & -uu_x - vu_y - P_x/\rho \\ 0 & 1 & -uv_x - vv_y - P_y/\rho \end{vmatrix}$$

ar.

$$\det[D] = \begin{vmatrix} u & v & w^2-a^2 \\ 1 & 0 & 0 \\ 0 & 1 & 0 \end{vmatrix}$$

Since the x and y axes are set tangent to a characteristic surface, the derivative w_z is indeterminate. A necessary and sufficient condition for the indeterminacy of w_z is det[D]=0 and det[N]=0. The first leads to $w_z = \pm a$ (the usual Mach cone), whereas the second yields the compatibility relation, where w is replaced by $\pm a$

$$a^2u_x + a^2v_y \mp a(vw_y + uw_x) + (vP_y + uP_x)/\rho = 0 \qquad (55)$$

When the y-axis is chosen to coincide with a generatrix of the Mach cone (a bicharacteristic), u vanishes and Equation (55) reduces to

$$a^2u_x + a^2v_y \mp avw_y + vP_y/\rho = 0$$

or

$$u_x + v_y \mp \cot\mu\, w_y + \frac{q\cos\mu}{\rho a^2} P_y = 0 \qquad (56)$$

Equation (56) is written in a local, characteristic-oriented coordinate system. For computational purposes, it is practical to relate it to a fixed spherical coordinate system, as shown in Figure 18. The y-axis is replaced by the L-axis in a bicharacteristic direction; the x and z axes, by two orthogonal axes N and M, respectively. For a small, but arbitrary, change of velocity ($\Delta q, \Delta\theta, \Delta\psi$) the corresponding change of velocity components Δu, Δv, and Δw along the N, L, and M axes is, to the first order of Δq, $\Delta\theta$, and $\Delta\psi$:

$$\Delta u = q\sin\delta\,\Delta\theta + q\sin\theta\cos\delta\,\Delta\psi$$

$$\Delta V = \cos\mu\,\Delta q - q\cos\delta\sin\mu\,\Delta\theta + q\sin\theta\sin\delta\sin\mu\,\Delta\psi$$

$$\Delta W = \pm\sin\mu\,\Delta q \pm q\cos\delta\cos\mu\,\Delta\theta \mp q\sin\theta\sin\delta\cos\mu\,\Delta\psi$$

The partial derivatives of u, v, w with respect to N or L have the same forms as given above; hence

$$\left.\begin{aligned} u_N &= q\sin\delta\,\theta_N + q\sin\theta\cos\delta\,\psi_N \\ V_L &= \cos\mu\,q_L - q\cos\delta\sin\mu\,\theta_L + q\sin\theta\sin\delta\sin\mu\,\psi_L \\ W_L &= \pm\sin\mu\,q_L \pm q\cos\delta\cos\mu\,\theta_L \mp q\sin\theta\sin\delta\cos\mu\,\psi_L \end{aligned}\right\} \quad (57)$$

Substituting Equation (57) into Equation (56), we finally obtain

$$\frac{1}{\rho a^2}P_L - \frac{\cos\delta}{\sin\mu\cos\mu}\,\theta_L + \frac{\sin\theta\sin\delta}{\sin\mu\cos\mu}\,\psi_L + \frac{1}{\cos\mu}(\sin\delta\,\theta_N + \sin\theta\cos\delta\,\psi_N) = 0 \quad (58)$$

where subscripts L, N denote partial differentiation; a is the speed of sound, ρ the density, μ the Mach angle, and δ is defined in Figure 18. Equation (49) is valid for either isoenergetic or nonisoenergetic flow; the difference is the constants of the Bernoulli equation. For the present application, air is assumed to be a perfect gas for which ρa^2 is equal to γP, where γ is the ratio of the specific heats.

Equation (58) and the Bernoulli equation are used to determine the supersonic flow field. A number of numerical schemes have been proposed for solving Equation (58). It can be shown that many of these schemes introduce difficulties into the solution by their methods of approximating Equation (58) in finite-difference form (Reference 8). However, in this work a simple form of the generalized finite-difference approximation presented in Reference 8 is used.

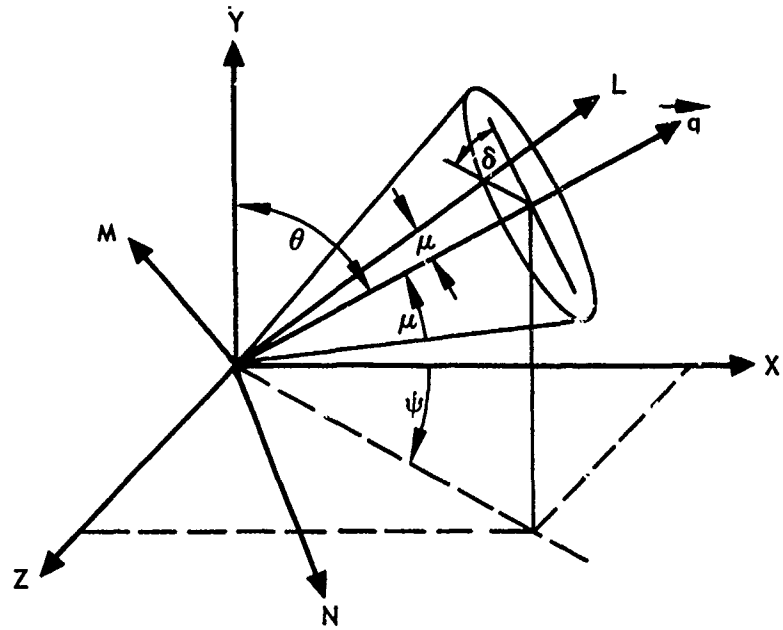

FIGURE 18. RELATION BETWEEN COORDINATE SYSTEMS

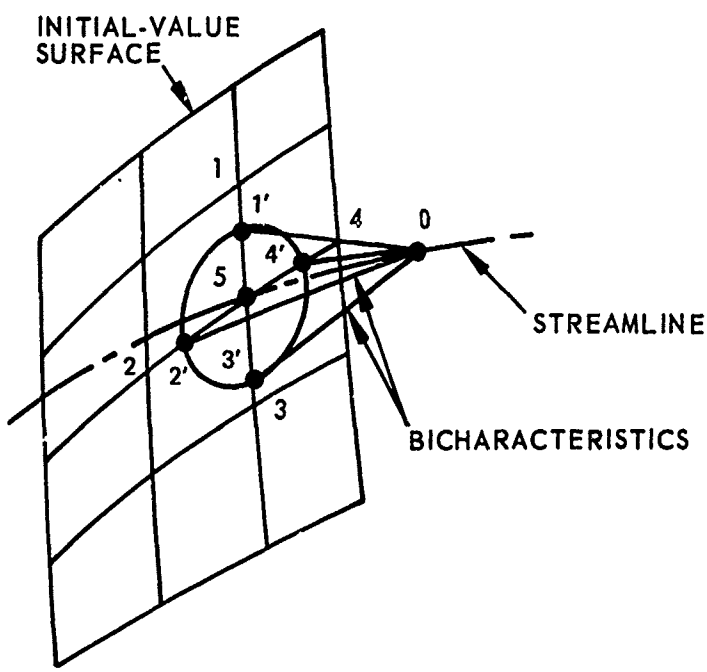

FIGURE 19. FIELD POINT COMPUTATION

c. Field Point Solution

This simple form of the generalized finite-difference approximation is illustrated by the field point solution shown in Figure 19. A field point is an interior point away from the boundaries. At such a point, given an initial value surface, Equation (58) in finite-difference form along three bicharacteristics passing through this point can be solved for P, θ, and ψ; however, in the present formulation, one more bicharacteristic is added for accuracy and numerical stability, as shown in Figure 19.

Thus, in finite-difference form, Equation (58) can be written

$$A_i P_0 + B_i \theta_0 + C_i \psi_0 = D_i \qquad \{i = 1,4\} \tag{59}$$

where

$$A_i = \sin\bar{\mu}\cos\bar{\mu}/(\gamma\bar{P})$$

$$B_i = -\cos\delta_i$$

$$C_i = \sin\bar{\theta}\sin\delta_i$$

$$D_i = A_i P_i + B_i \theta_i + C_i \psi_i - (\sin\delta_i \theta_N + \sin\bar{\theta}\cos\delta_i \psi_N)\sin\bar{\mu}\Delta L_i$$

and the double summation convention is not used in D_i. The barred quantities are average properties between points i and 0, and L_i is the distance between points i and 0; δ_i is calculated using the average flow direction between points i and 0 (see discussion in subsection 2. c). As in Reference 8 we define a residual function

$$\bar{R}^2 = \sum_{i=1}^{4} (A_i P_0 + B_i \theta_0 + C_i \psi_0 - D_i)^2$$

and seek a solution for P_0, θ_0, and ψ_0 that minimizes the residual function $\bar{R}^2$. Differentiating $\bar{R}^2$ with respect to P_0, θ_0, and ψ_0, and setting the results equal to zero yields

$$\left.\begin{aligned} P_o\sum_{i=1}^{4}A_i^2 + \theta_o\sum_{i=1}^{4}A_iB_i + \psi_o\sum_{i=1}^{4}A_iC_i &= \sum_{i=1}^{4}A_iD_i \\ P_o\sum_{i=1}^{4}A_iB_i + \theta_o\sum_{i=1}^{4}B_i^2 + \psi_o\sum_{i=1}^{4}B_iC_i &= \sum_{i=1}^{4}B_iD_i \\ P_o\sum_{i=1}^{4}A_iC_i + \theta_o\sum_{i=1}^{4}B_iC_i + \psi_o\sum_{i=1}^{4}C_i^2 &= \sum_{i=1}^{4}C_iD_i \end{aligned}\right\} \quad (60)$$

which can then be solved for P_o, θ_o, and ψ_o.

d. Body Point Solution

A body point is a point on the surface of the fuselage. At such a point, as shown in Figure 20, the flow must be tangent to the surface; hence at the new body point 0

$$l_b \sin\theta_o \cos\psi_o + m_b \cos\theta_o + n_b \sin\theta_o \sin\psi_o = 0 \quad (61)$$

where (l_b, m_b, n_b) are the direction cosines of the normal vector to the surface at the new point. Since the tangency condition (61) relates the flow angles θ_o and ψ_o, two bicharacteristics are sufficient for determining P_o, θ_o, and ψ_o. However,

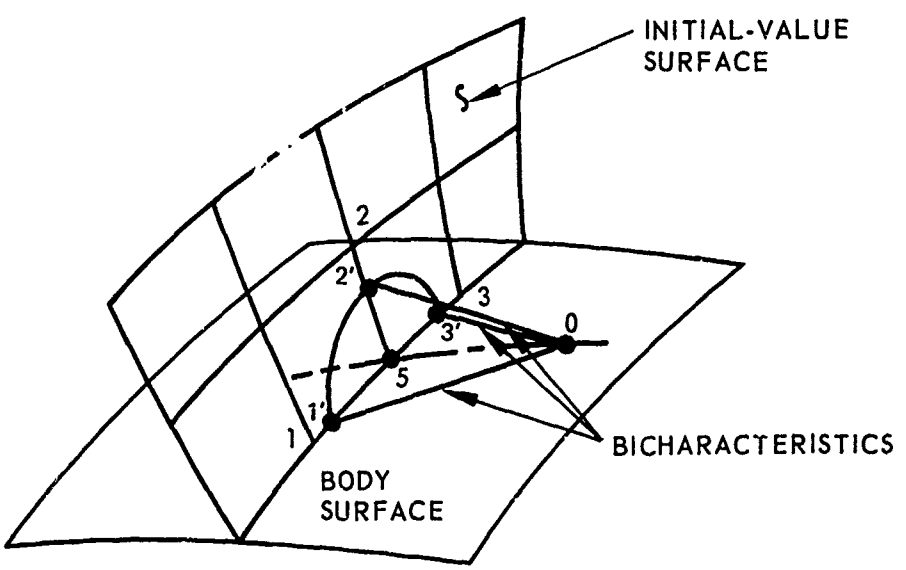

FIGURE 20. BODY POINT COMPUTATION

it is apparent from Figure 20 that three bicharacteristics are available and the choice of a specific pair will have a strong influence on the results; thus the addition of a third bicharacteristic is both natural and desirable.

This then becomes an extremal problem with the tangency condition (61) as a constraint. The original procedure was to differentiate the residual function $\overline{R}^2$ with respect to P_o and ψ_o, considering θ_o as an implicit function of ψ_o through Equation (61), and then set the results to zero. This led to a transcendental equation which had to be solved by an iterative process. In the early stage of revision of the 3DMoC program, this process occasionally led to an unwanted root. This difficulty was circumvented by a new approach which, in effect, reduces the nonlinear equations to linear ones. Indeed, if we consider the special case $m_b = 1$, we obtain the desired solution $\theta = \pi/2$ from Equation (61) immediately. The finite-difference forms of Equation (58) along three bicharacteristics are then

$$A_i P_o + C_i \psi_o = D_i - \frac{\pi}{2} B_i \qquad \{i = 1,3\}$$

and the minimization of the residual function

$$\overline{R}^2 = \sum_{i=1}^{3} (A_i P_o + C_i \psi_o - D_i + \frac{\pi}{2} B_i)^2$$

leads to the following equations which are linear in P_o and ψ_o:

$$P_o \sum_{i=1}^{3} A_i^2 + \psi_o \sum_{i=1}^{3} A_i C_i = \sum_{i=1}^{3} A_i D_i - \frac{\pi}{2} \sum_{i=1}^{3} A_i B_i$$

$$P_o \sum_{i=1}^{3} A_i C_i + \psi_o \sum_{i=1}^{3} C_i^2 = \sum_{i=1}^{3} C_i D_i - \frac{\pi}{2} \sum_{i=1}^{3} B_i C_i$$

These can readily be solved for P_o and ψ_o. For the general case, $m_b = 1$, the same analysis applies after rotating the local coordinates[2] to make $m_b = 1$. After the solution is obtained in terms of the velocity components u, v, w, and the pressure P, the solution is rotated back into the original coordinate system.

[2] Since Equation (50) relates the pressure P to the local flow angles θ and ψ, it can be solved using any suitably chosen local coordinates.

e. Shock Point Solution

While the field or body point is calculated along a streamline, the shock point is calculated along a two-dimensional-shock line[3], as shown in Figure 21. At a point on the shock, the flow must satisfy the oblique shock relation

$$\tan \Delta_o = \left(\frac{\xi_o - 1}{\gamma M_\infty^2 - \xi_o + 1}\right)\left[\frac{2\gamma M_\infty^2 - (\gamma-1) - (\gamma+1)\xi_o}{(\gamma+1)\xi_o + (\gamma-1)}\right]^{1/2} \qquad (62)$$

where Δ_o is the flow deflection angle across the shock wave and $\xi_o = P_o/P_\infty$ is related to θ_o and ψ_o through

$$l_s \sin\theta_o \cos\psi_o + m_s \cos\theta_o + n_s \sin\theta_o \sin\psi_o = \cos\Delta_o \qquad (63)$$

where (l_s, m_s, n_s) are the direction cosines of the freestream velocity vector.

This again is an extremal problem with a constraint $C(P_o, \theta_o, \psi_o) = 0$, given parametrically by Equations (62) and (63). In the original program the usual procedure of minimizing the residual function led to simultaneous nonlinear equations which were difficult to solve, even numerically. However, by applying the same technique of choosing appropriate coordinates, the set of simultaneous nonlinear equations can be reduced to a single transcendental equation, as is shown below.

When the angle of attack is zero, the freestream direction is aligned with the Y-axis. In this special case, $m_s = 1$, and $\theta_o = \Delta_o$ is the desired solution of Equation (63); the constraint reduces to

$$\tan\theta_o = \left(\frac{\xi_o - 1}{\gamma M_\infty^2 - \xi_o + 1}\right)\left[\frac{2\gamma M_\infty^2 - (\gamma-1) - (\gamma+1)\xi_o}{(\gamma+1)\xi_o + (\gamma-1)}\right]^{1/2} \qquad (64)$$

relating $\xi_o = P_o/P_\infty$ to θ_o only. Three bicharacteristics are used for the shock point solution, as shown in Figure 21, and Equation (58) assumes the finite-difference form

[3]A plane that contains the freestream velocity vector and the downstream velocity vector at a shock point is called a "two-dimensional-shock plane" (Figure 21b). On the shock surface, a line that is everywhere tangent to the two-dimensional-shock planes is called a "two-dimensional-shock line".

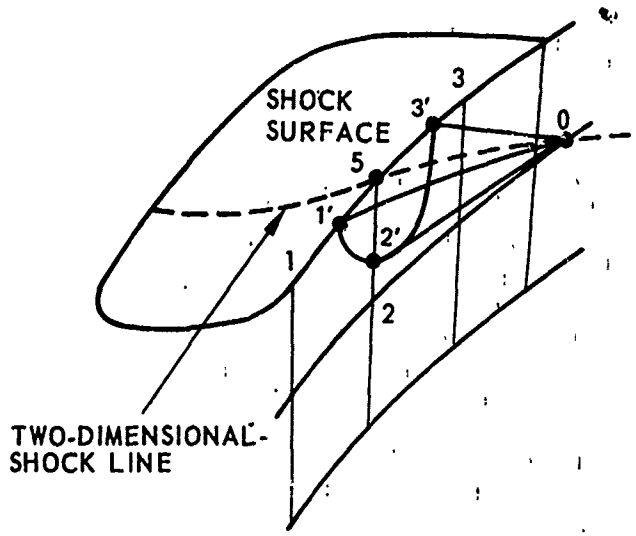

(a)

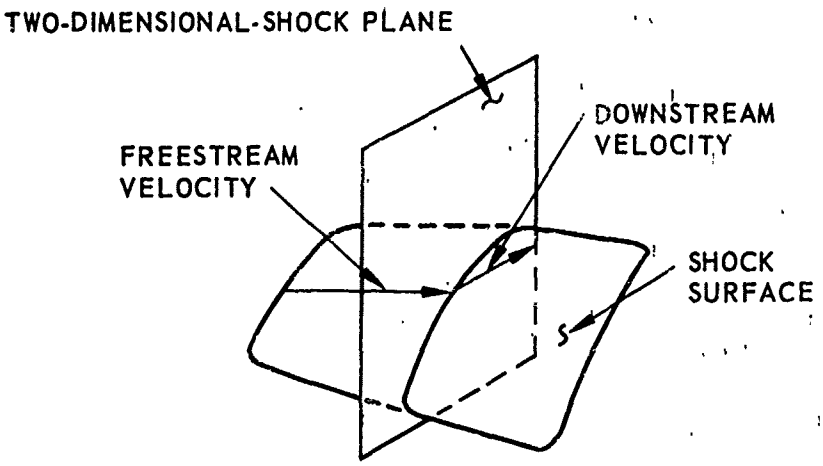

(b)

FIGURE 21. TWO-DIMENSIONAL-SHOCK PLANE AND SHOCK POINT COMPUTATION

$$A_i P_o + B_i \theta_o + C_i \psi_o = D_i \qquad \{i = 1,3\}$$

where A_i, B_i, C_i and D_i are given in Equation (50). Again we minimize the residual function

$$\bar{R}^2 = \sum_{i=1}^{3} (A_i P_o + B_i \theta_o + C_i \psi_o - D_i)^2$$

by differentiating it with respect to P_o and ψ_o, considering θ_o as a function of P_o through Equation (64), and setting the results to zero to obtain

$$\sum_{i=1}^{3} (A_i + B_i \, d\theta/dP)(A_i P_o + B_i \theta_o + C_i \psi_o - D_i) = 0 \qquad (65)$$

$$P_o \sum_{i=1}^{3} A_i C_i + \theta_o \sum_{i=1}^{3} B_i C_i + \psi_o \sum_{i=1}^{3} C_i^2 - \sum_{i=1}^{3} C_i D_i = 0 \qquad (66)$$

Equations (64), (65), (66) are solved for P_o, θ_o, and ψ_o; substitution of Equations (64) and (66) into (65) leads to a transcendental equation for P_o alone, which is then solved by the Newton-Raphson method. When the angle of attack is not zero, the coordinates are rotated until the local Y-axis is aligned with the freestream velocity. This makes $m_s = 1$ and the same analysis holds. After the solution has been obtained in terms of the velocity components u, v, w, and the pressure P, the solution is simply rotated back into the original coordinate system.

2. NUMERICAL PROCEDURES

a. Constant Body Station Data Surfaces

In the original program, computation proceeded along outgoing bicharacteristics and streamlines. One drawback of such a characteristic network is that the data surfaces become more and more distorted as the computation proceeds downstream. Eventually the distortion (or warping) of the data surfaces makes their use impractical. This happens much sooner in highly three-dimensional flows. These warped surfaces also make the interpolation of data or rearrangement of data points fairly complicated, as many interpolative operations in three dimensions must be made.

In the new program, constant body station data surfaces (Y=constant) are used. Each data surface consists of a number of data rings, with the first data ring on the body and the last data ring on the shock. All data rings have the same number of data points.

The advantages of the new network are:

1. Data interpolation is simple and two-dimensional.
2. Rearrangement of data points (which is essential even in moderately three-dimensional flow) becomes practical because of simpler interpolation.
3. The Courant-Friedrichs-Lewy (CFL) stability condition can be readily applied because the network is two-dimensional and more regular.
4. The extent of flow field to be computed can be easily determined; one does not have to figure out where to begin the right running characteristics or how far a particular characteristic will reach.
5. The mesh size is more uniform, unlike in the old program where the distance between two adjacent data points may become unusually large because of warping of the characteristic network.
6. The geometric normal to the shock surface is simple to compute and this makes the important shock drift control practical.

b. Base Point Location

Referring to Figure 19, points 1 to 5 are the data points to be used for computing point 0 on the new data surface. Points 1' to 4' are the base points, which are the intersections of the backward-facing Mach conoid with the data lines. To find the location of a base point is one of the basic operations of the 3DMoC program.

The location of a base point was an involved and sometimes troublesome operation in the original program. The coordinates were rotated to a local system before the intersections of the data lines with the Mach cone were determined. The correct choice of one intersection was made and the coordinates were rotated back to the original system. No general logic was available to guide the choice of the intersection, which sometimes caused trouble. The new method described below has made possible a simple, direct, and unequivocal determination of the base point location in the new program.

Figure 22 shows data points 1, 2, 4, and 5 in the upstream surface, and the new point being calculated, denoted by 0. The vector from 5 to 2 is $\vec{a}$ and the

vector from 5 to the unknown base point 2' is $\vec{x}$. Point 5 is the origin of the streamline through point 0, and is called the hub point in the following discussion.

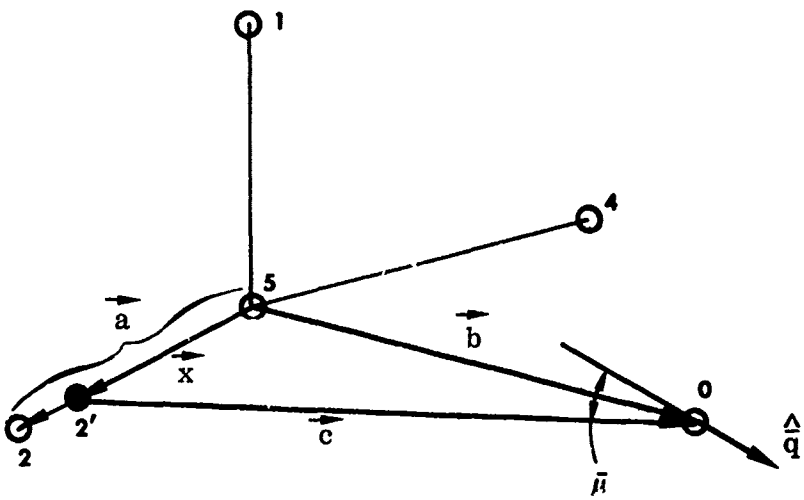

FIGURE 22. GEOMETRY FOR BASE POINT SOLUTION

Let $\vec{x} = L\vec{a}$, where L = x/a is an unknown to be determined. In Figure 22 the vector $\vec{c}$ is defined by

$$\vec{c} = \vec{b} - \vec{x} = \vec{b} - L\vec{a} \tag{67}$$

Let $\hat{q}$ be the unit vector in the average flow direction and $\bar{\mu}$ be the average Mach angle between points 2' and 0; then

$$\cos\bar{\mu} = \frac{\vec{c}\cdot\hat{q}}{c} = \frac{(\vec{b}-L\vec{a})\cdot\hat{q}}{\sqrt{(\vec{b}-L\vec{a})\cdot(\vec{b}-L\vec{a})}} \tag{68}$$

or

$$(b^2 - 2\vec{a}\cdot\vec{b}\,L + a^2L^2)\cos^2\bar{\mu} = (\vec{b}\cdot\hat{q} - \vec{a}\cdot\hat{q}\,L)^2 \tag{69}$$

which is the same as

$$AL^2 - 2BL + C = 0 \tag{70}$$

where

$$A = a^2\cos^2\bar{\mu} - (\vec{a}\cdot\hat{\vec{q}})^2$$

$$B = \vec{a}\cdot\vec{b}\cos^2\bar{\mu} - (\vec{a}\cdot\hat{\vec{q}})(\vec{b}\cdot\hat{\vec{q}})$$

$$C = b^2\cos^2\bar{\mu} - (\vec{b}\cdot\hat{\vec{q}})^2$$

The roots are

$$L = \frac{C}{B \pm \sqrt{B^2 - AC}} \tag{71}$$

The following is a summary of the logic for the choice of the correct root.

I. If A>0, the vector defined by $\vec{a}$ intersects both sides of the forward-facing Mach cone. Two subcases must be considered.

(1) If C<0, the hub point (point 5 in Figure 22) lies inside the Mach cone. The positive root is the desired one, and corresponds to the use of the negative sign in the expression above.

(2) If C>0, the hub point lies outside the Mach cone, and two subcases are possible.

(a) If B<0, there are two negative roots. The larger root is the desired one, and corresponds to the use of the negative sign.

(b) If B>0, there are two positive roots. Again the larger root is the desired one, and therefore the negative sign is used.

II. If A<0, the vector defined by $\vec{a}$ intersects one side of the forward-facing Mach cone and other side of the backward-facing Mach cone. Two subcases exist.

(1) If C<0, the hub point lies inside Mach cone, and two subcases must be considered.

(a) If B<0, there are two positive roots. The smaller root is wanted. Therefore the negative sign is used.

(b) If B>0, there are two negative roots. Neither root is acceptable. A failure message should be printed and the calculation terminated.

(2) If C>0, the hub point lies outside the Mach cone. There are two subcases.

(a) If B<0, the negative root is wanted. Therefore the negative sign is used.

(b) If B>0, neither root is acceptable. A failure message should be printed and the calculation terminated.

III. If A = 0, the vector defined by $\vec{a}$ intersects only one side of the forward Mach cone. The same subcases exist as in II (i.e., take the negative sign) with the exception that there is only one root.

Therefore, except when A<0 and B>0 (which requires the selection of another data line), the negative sign is always used. Extrapolation occurs when L is not in the interval (0, 1). With the factor L available, interpolation for data at the base point is simple. For instance, the pressure $P_{2'}$ at point 2' is given by

$$P_{2'} = P_5 + L(P_2 - P_5) \tag{72}$$

c. Basic Solution Procedure

The numerical solution is carried out in a series of data surfaces which are perpendicular to the Y-axis. Given an initial value surface, flow properties are computed at points on the next surface through an iterative procedure, following streamlines for the body and field points or following two-dimensional-shock lines for the shock points.

This procedure is illustrated by the field point computation. Referring to Figure 19, the location of the new field point, point 0, is determined by use of the average flow direction between point 0 and the field point on the previous data surface, point 5. In the first iteration, the properties at point 0 are assumed to be the same as those at point 5. Then the location of the base points 1' to 4' and the flow properties at these points are determined by the procedure described in the preceding subsection 2.b.

After the four base points are located, corresponding to assumed properties at the new point 0, the coefficients A_i, B_i, C_i, and D_i in Equation (59) are evaluated. The angle δ_i (see Figure 18) is determined by

$$\cos\delta_i = (\hat{\vec{q}}_i \times \hat{j} \cdot \vec{N})(\|\hat{\vec{q}}_i \times \hat{j}\| N)^{-1} \tag{73}$$

where $\vec{N} = \hat{\vec{q}}_i \times \vec{L}$; $\sin\delta_i$ is given by

$$\sin\delta_i = \pm(1 - \cos^2\delta_i)^{1/2} \tag{74}$$

which takes the same sign as that of $\vec{L} \cdot (\hat{\vec{q}}_i \times \hat{j})$. The derivatives θ_N and ψ_N are

obtained from

$$\theta_N = \nabla\theta \cdot \hat{N}$$
$$\psi_N = \nabla\psi \cdot \hat{N}$$

The computation of $\nabla\theta$ and $\nabla\psi$ can be illustrated by evaluating $\nabla\theta$ for the first bicharacteristic. We note that

$$\left.\begin{aligned}
\theta_o - \theta_{2'} &= \frac{\partial\theta}{\partial X}(X_o - X_{2'}) + \frac{\partial\theta}{\partial Y}(Y_o - Y_{2'}) + \frac{\partial\theta}{\partial Z}(Z_o - Z_{2'}) \\
\theta_o - \theta_{1'} &= \frac{\partial\theta}{\partial X}(X_o - X_{1'}) + \frac{\partial\theta}{\partial Y}(Y_o - Y_{1'}) + \frac{\partial\theta}{\partial Z}(Z_o - Z_{1'}) \\
\theta_o - \theta_{4'} &= \frac{\partial\theta}{\partial X}(X_o - X_{4'}) + \frac{\partial\theta}{\partial Y}(Y_o - Y_{4'}) + \frac{\partial\theta}{\partial Z}(Z_o - Z_{4'})
\end{aligned}\right\} \quad (75)$$

which are solved for $\frac{d\theta}{dX}$, $\frac{d\theta}{dY}$, and $\frac{d\theta}{dZ}$, the three components of $\nabla\theta$.

Having evaluated the coefficients A_i, B_i, C_i, and D_i we solve Equation (60) for the properties P_o, θ_o, and ψ_o, which are then used to relocate the new field point and the corresponding base points for restarting the iteration. This process is repeated until the difference between two successive iterations is less than a specified value for each of the quantities P_o, θ_o, and ψ_o. Body points and shock points are computed in an analogous way.

d. Interpolation of Data at a Base Point

In the original program, a second order Lagrange interpolation was used to determine the flow properties at a base point. At an inflection point on a plot of a certain property versus distance, such an interpolation procedure leads to different values of the property at the same abscissa, depending upon the trio of base points used, as shown in Figure 23.

In Figure 23, it can be easily seen that the different values PP_1 and PP_2 are obtained by interpolating, using three points centered on point O_1 in one case, and on point O_2 in the other. This discrepancy was responsible for some of the troubles encountered in the original program. In the new program, linear interpolation is used to determine the properties at a base point. Comparison of numerical results with experimental data has shown that this simple interpolation is satisfactory.

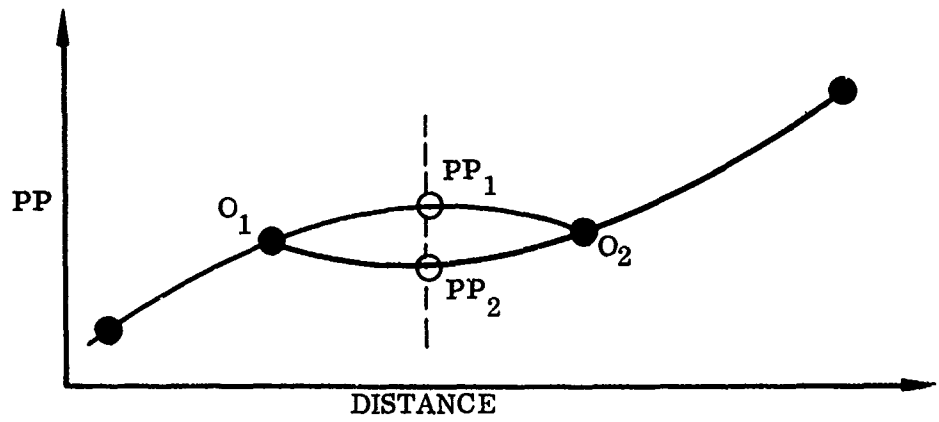

FIGURE 23. INFLECTION POINT IN THE DATA

Accuracy can be improved by decreasing the mesh size. Since a great number of iterations for properties at the base points are required in the flow field computation, the increase in computing time due to the increased number of data points is offset by the decrease in computing time due to the simplicity of interpolation.

e. Step Size Control

The Courant-Friedrichs-Lewy (CFL) stability condition, which states that the domain of dependence of the difference equation must contain the domain of dependence of the differential equation, is generally used in numerical integration of hyperbolic equations. Since the data surface will be flat and the network fairly regular, the CFL condition can be applied easily. In the base point computation the position of each base point will be checked for satisfaction of the CFL condition. This is simply done by noting whether the factor L (see base point computation) is less than $1/\sqrt{2} \approx 0.7$. If this condition is satisfied at every base point on the data surface, the step size will be increased by 5%; otherwise, the step size will be decreased by 10%.

The new program also allows changes in the grid size by assigning different numbers of data points in different flow regions. The total number of data points per data ring can be assigned for data surfaces between two Y values. In addition, the lateral grid size can be halved between two assigned data points along a data ring. It was found very useful to halve the grid size in regions of high lateral gradients, or high rates of change of gradients, such as the region near the leading edge of a wing.

Notice that the longitudinal step size is influenced by the lateral grid size through the CFL condition. Therefore, by assigning the number of data points and the use of the half-size grid, the downstream step size can be controlled indirectly.

f. Respacing of Data Points

Since the network of data points is built up following streamlines, and streamlines tend to converge on the lee side of bodies, the data points tend to crowd together in the same region after a number of steps. Since the CFL condition has to be satisfied everywhere, this region determines the step size. Even in a moderately three-dimensional flow, the step size may be seriously reduced after a certain number of steps, and a rearrangement of data points becomes necessary. In the new program, the flat data surface makes rearranging data points practical. Cubic spline interpolation is used to rearrange the data points twice: once along the data ring (i.e., in the circumferential direction), and once across the data rings (i.e., in the radial direction). Rearranging data points helps in the numerical stability of the computation, and also results in a more even distribution of data points and hence better accuracy.

As the distance between the shock and the body increases, the distance between two data rings becomes much greater than the distance between two data points. When this condition prevails at every shock point, the program will automatically introduce an additional data ring as the data points are being respaced.

g. Shock Point Drift Control

In three-dimensional supersonic inviscid flow computations the shock wave is a free boundary to be determined during the computation. As such, it is subject to drifting. Experience has shown that, as the number of steps increases, the shock normal determined from the local flow properties gradually deviates from the geometric shock normal until a failure occurs. This shock point drift is shown schematically in Figure 24.

In the new program, subroutine HARNES is used to control the shock point drift. After a shock ring has been calculated, the shock normals determined from the flow properties are averaged with the geometric shock normals at every shock point. The average normals are then used to recompute the flow properties at the shock points. Experience has shown that, although the average normal differs

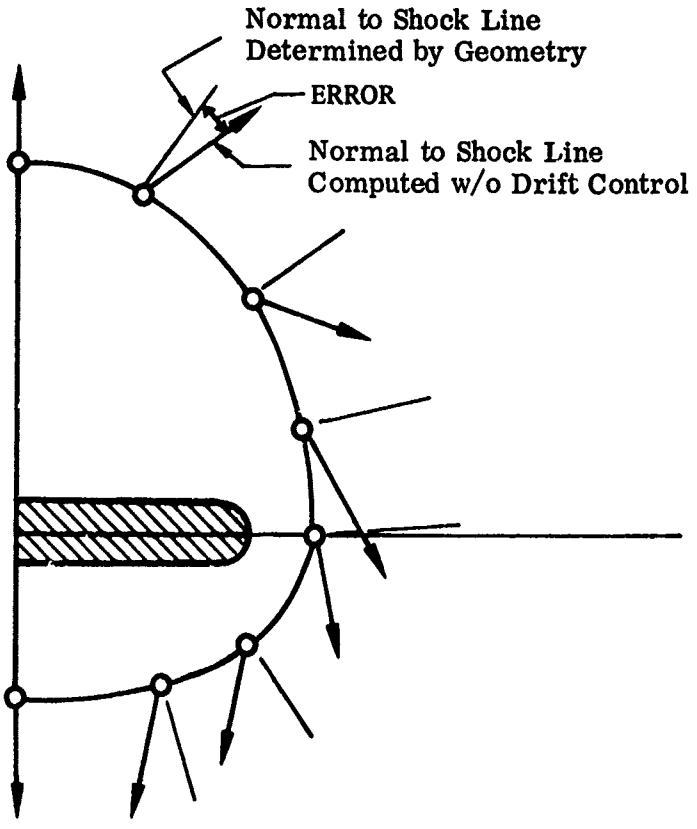

FIGURE 24. SHOCK POINT DRIFT

only slightly from either of the normals (which justifies the use of the average normal), the shock point drift is effectively checked.

h. Calculation of θ_N and ψ_N for the Field Point

In the original program, a least squares process was used to obtain the average gradients for θ and ψ, using the values of θ and ψ at all four base points and the new point. The quantities θ_N and ψ_N at each base point were then evaluated using these average gradients. Since, ideally, the local gradients of θ and ψ, averaged along a given bicharacteristic, should be used to evaluate θ_N and ψ_N, the process using only one set of average gradients for the entire Mach cone is inaccurate. In the new program, the local gradients of θ and ψ are obtained using only three of the base points and the new point for each bicharacteristic, as illustrated by Equation (75). Thus each bicharacteristic has its own $\nabla\theta$ and $\nabla\psi$ values to be used in forming θ_N and ψ_N.

i. Treatment of Undefined δ and ψ

The direction of the local velocity is defined by the angles θ and ψ, while the direction of a bicharacteristic is defined by the angle δ (see Figure 18). The angles δ and ψ become undefined when the local velocity vector is aligned with the Y-axis (i.e., $\theta = 0$).

In the original program for computing the flow field over a slab delta wing, this occurred on the flat surface at the plane of symmetry and was "fixed" by replacing the flat center section by a wedge slope of 0.01^{o}. While this fix was satisfactory for the slab delta wing, it was not a general solution to the problem. In the new program, a built-in logic package rotates the X and Y axes counter clockwise around the Z-axis through 0.1 radian when the program detects a small value of θ. The rotation could be repeated, when called forth by a small value of θ, as many as 16 times. This device has worked very well.

SECTION V

RESULTS

Both the IVS program and the 3DMoC program have been tested on a number of flow field computations. The results of two test cases are presented here. The first case is the flow of helium over a blunted cone of 15° half-angle at Mach 14.9 and 20° angle of attack. The second case is the flow field about a slab delta wing of 70° sweep at Mach 9.6 and 15° angle of attack. In both cases, good agreement between computed results and available experimental data was obtained.

1. BLUNTED CONE AT LARGE ANGLE OF ATTACK

To test the program's ability to handle large angles of attack, the first test case is the flow over a blunted cone of 15° half-angle at 20° angle of attack. The freestream Mach number is 14.9 and the medium is helium, which has a ratio of specific heats of 1.6667. This is a severe test case, since the lee side of the cone lies completely in the shadow region of the freestream.

The body description of a cone is very simple. Since the cone is a slab delta wing without the flat sections, the same body description subroutine was used. About six minutes of CPU time were needed on the CDC 6600 computer for calculating the flow field to 75 nose radii downstream.

The computed shock shape is shown in Figure 25, and is compared with the experimental data of Reference 9. The agreement is very good. Reference 9 also presents the flow field calculations of Reference 10 which failed at about 10 nose radii downstream. Envelope shocks may occur on the lee side, but in this case they are apparently very weak and the present method is capable of calculating right through them without special treatment. Figure 26 is a comparison of the calculated pressure with both experimental data (Reference 9) and other calculated data (Reference 10). No essential disagreement exist between the two methods up to 10 nose radii downstream, as both agree quite well with the experimental data. However, on the lee side, the present method is not restricted in its downstream extent.

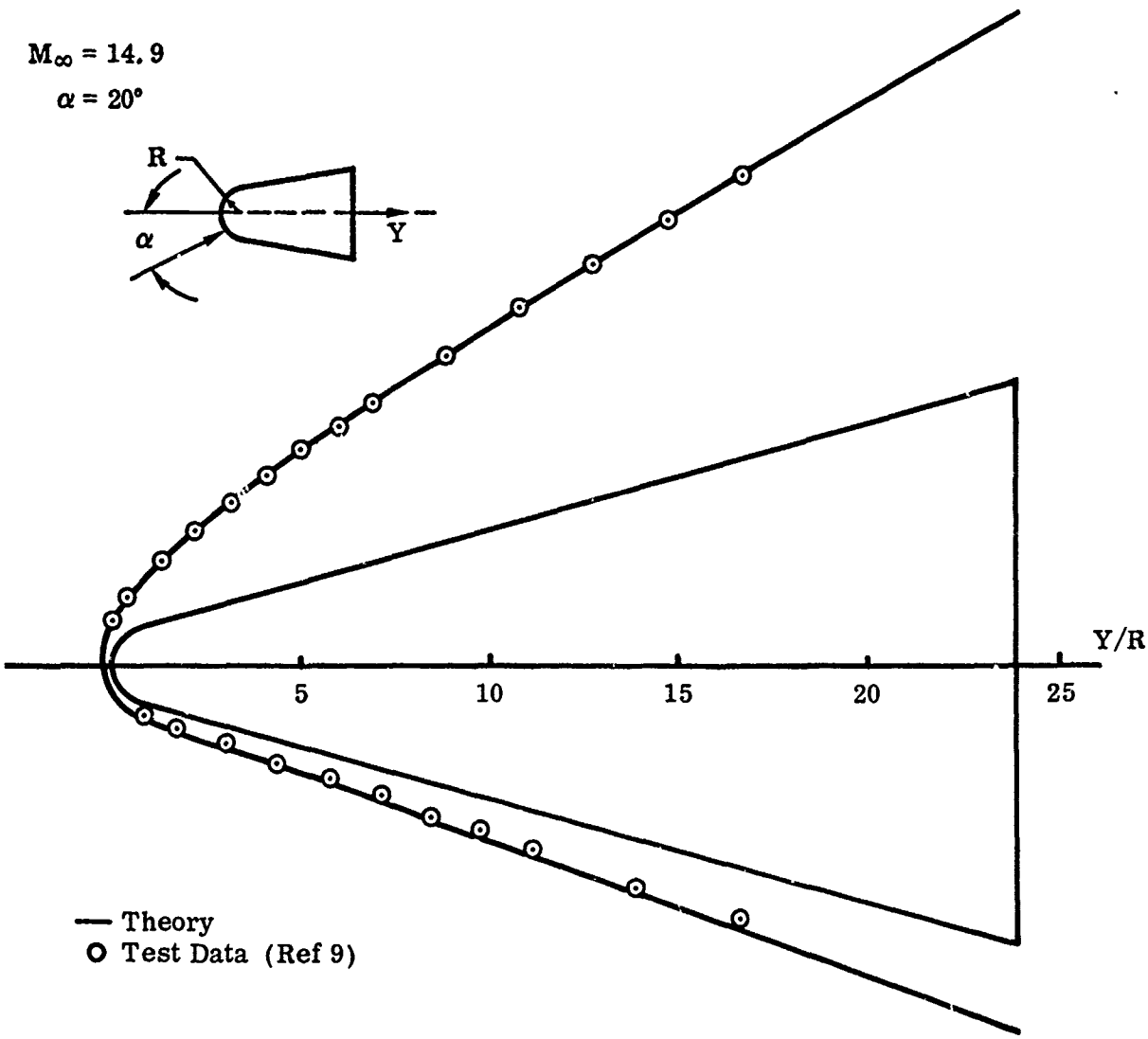

FIGURE 25. SIDE VIEW OF THE BOW SHOCK ON A BLUNTED 15° CONE AT 20° ANGLE OF ATTACK

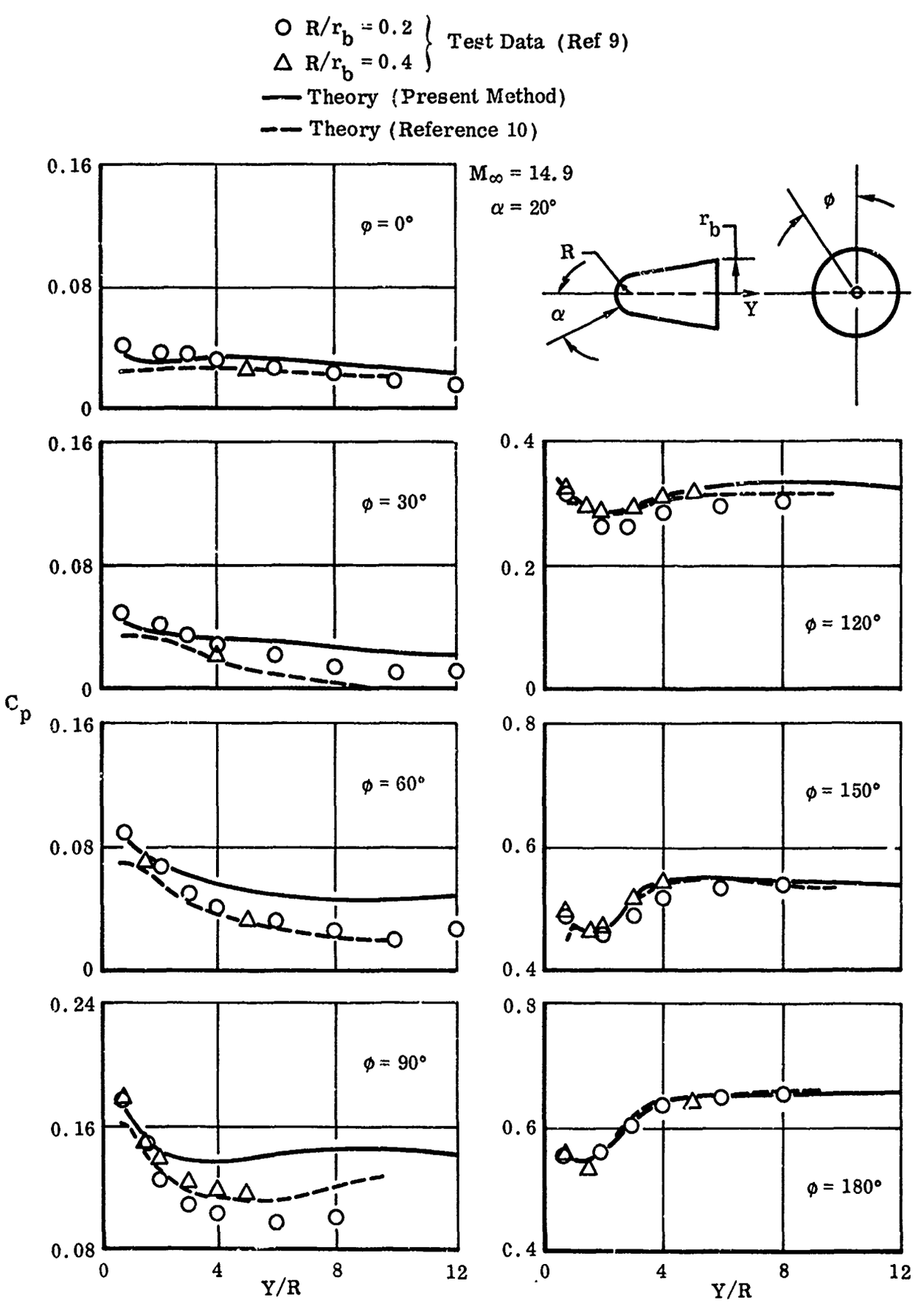

FIGURE 26. PRESSURE DISTRIBUTION ON A BLUNTED 15° CONE AT 20° ANGLE OF ATTACK

2. SLAB DELTA WING AT ANGLE OF ATTACK

The second test case is the flow field around a spherically-capped 70° sweep slab delta wing with cylindrical leading edges at Mach 9.6 and 15° angle of attack. The computation was carried out to 12.5 nose radii downstream, with a CPU time requirement of about three minutes on the CDC 6600 computer. Experimental data were obtained from Bertram's work (Reference 11) for M = 9.6 in air. Figure 27 shows the profile and the front views of the calculated bow shock supported by the slab delta wing. The cross section is smooth and convex everywhere. Figure 28 shows the plan view of the shock surface. Note that the shock wave has a point of inflection near the last calculated station. This means that, somewhat further downstream, the bow shock will bend away from the leading edge. This phenomenon can be seen in Schlieren photographs of Reference 11.

The centerline pressure distribution on the windward surface is compared with experimental data in Figure 29. The agreement is very good. Figure 30 compares pressure distributions along planes normal to the wing's leading edge with experimental data. The abscissa is the ratio of distance along the surface to wing thickness. The positive values of S/t refer to the windward side; the negative values, to the lee side. Very good agreement is seen, although the quality begins to decay on the expansion surface near the leading edge toward the end of the wing. This could be due to viscous effects. Nevertheless, fairly good pressure data agreement is obtained on the lee side of the wing (negative S/t), even though the present numerical method does not account for vortices which exist in the real flow.

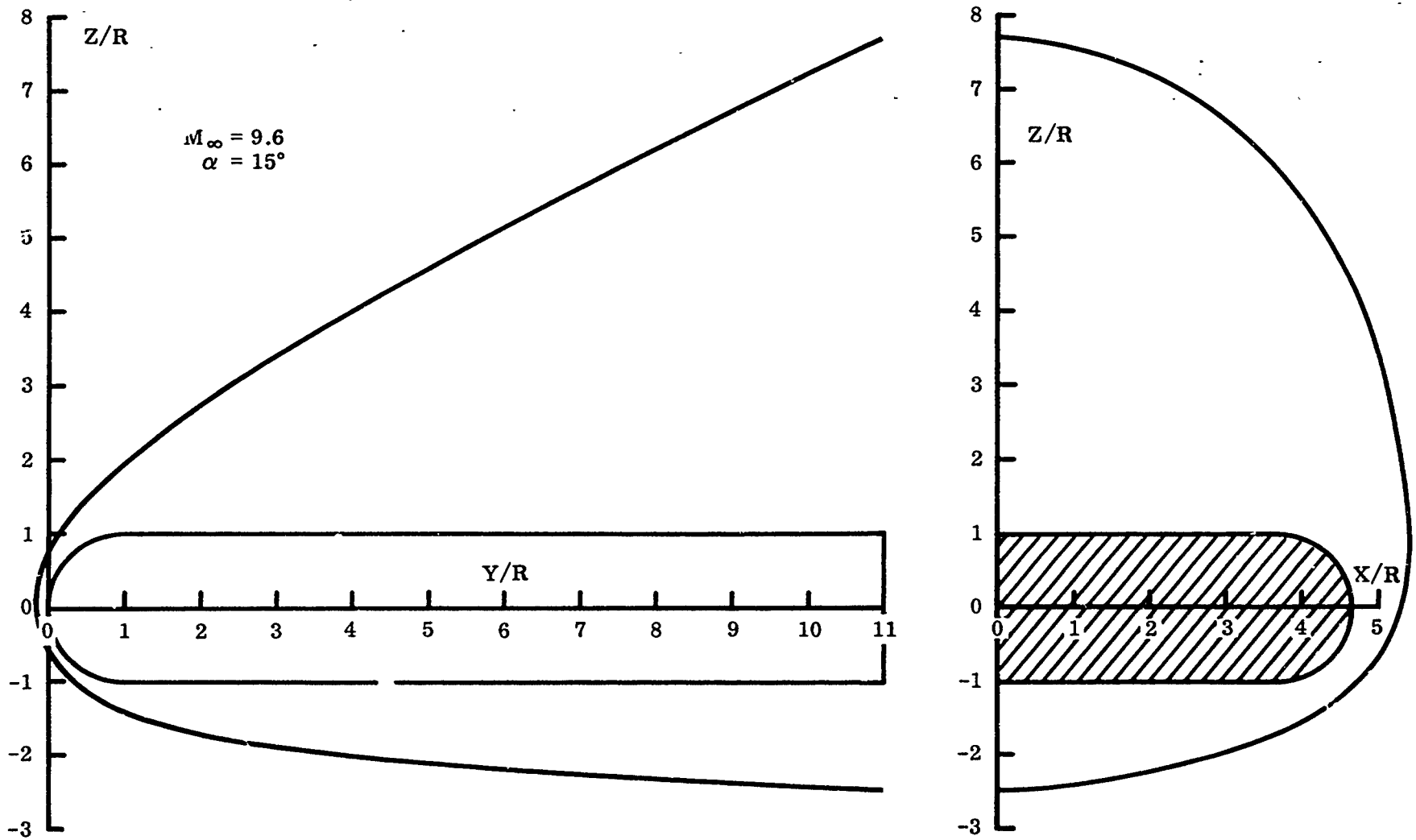

FIGURE 27. BOW SHOCK ON A SPHERICALLY-NOSED SLAB DELTA WING WITH 70° SWEEP

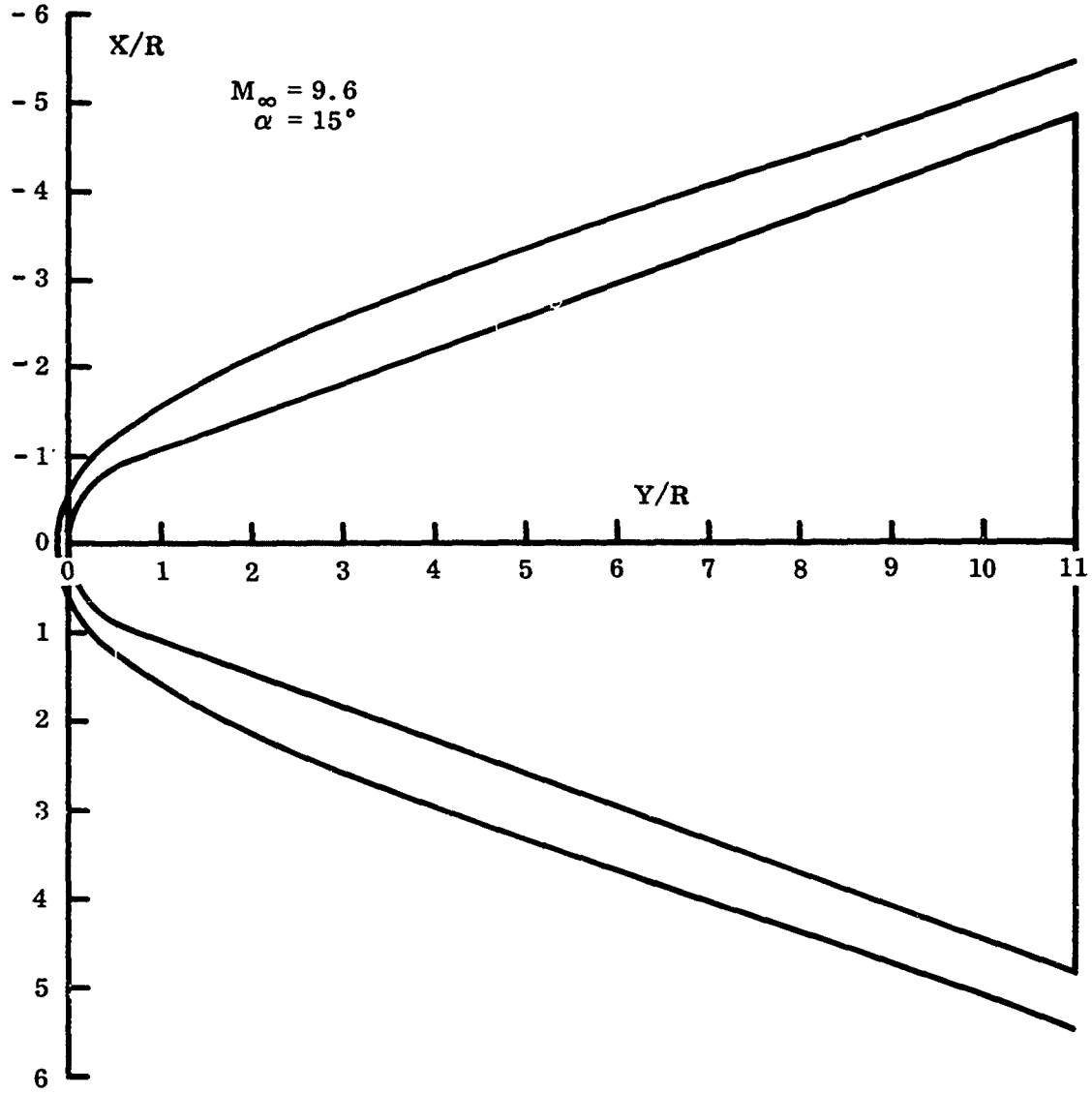

FIGURE 28. TOP VIEW OF BOW SHOCK ON A SPHERICALLY-NOSED SLAB DELTA WING WITH 70° SWEEP

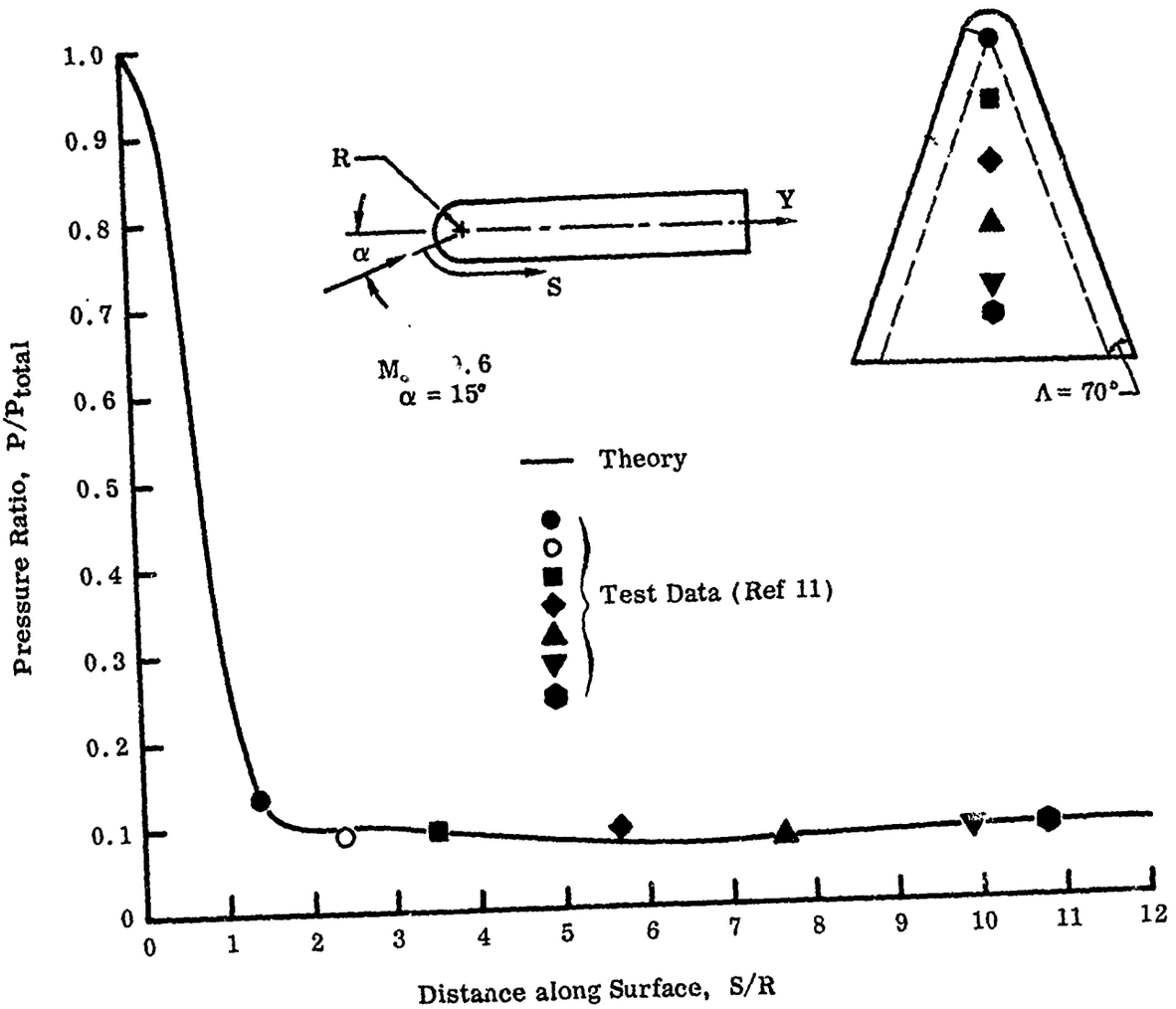

FIGURE 29. CENTERLINE PRESSURE DISTRIBUTION ON WINDWARD SURFACE OF A SPHERICALLY-NOSED SLAB DELTA WING WITH 70° SWEEP

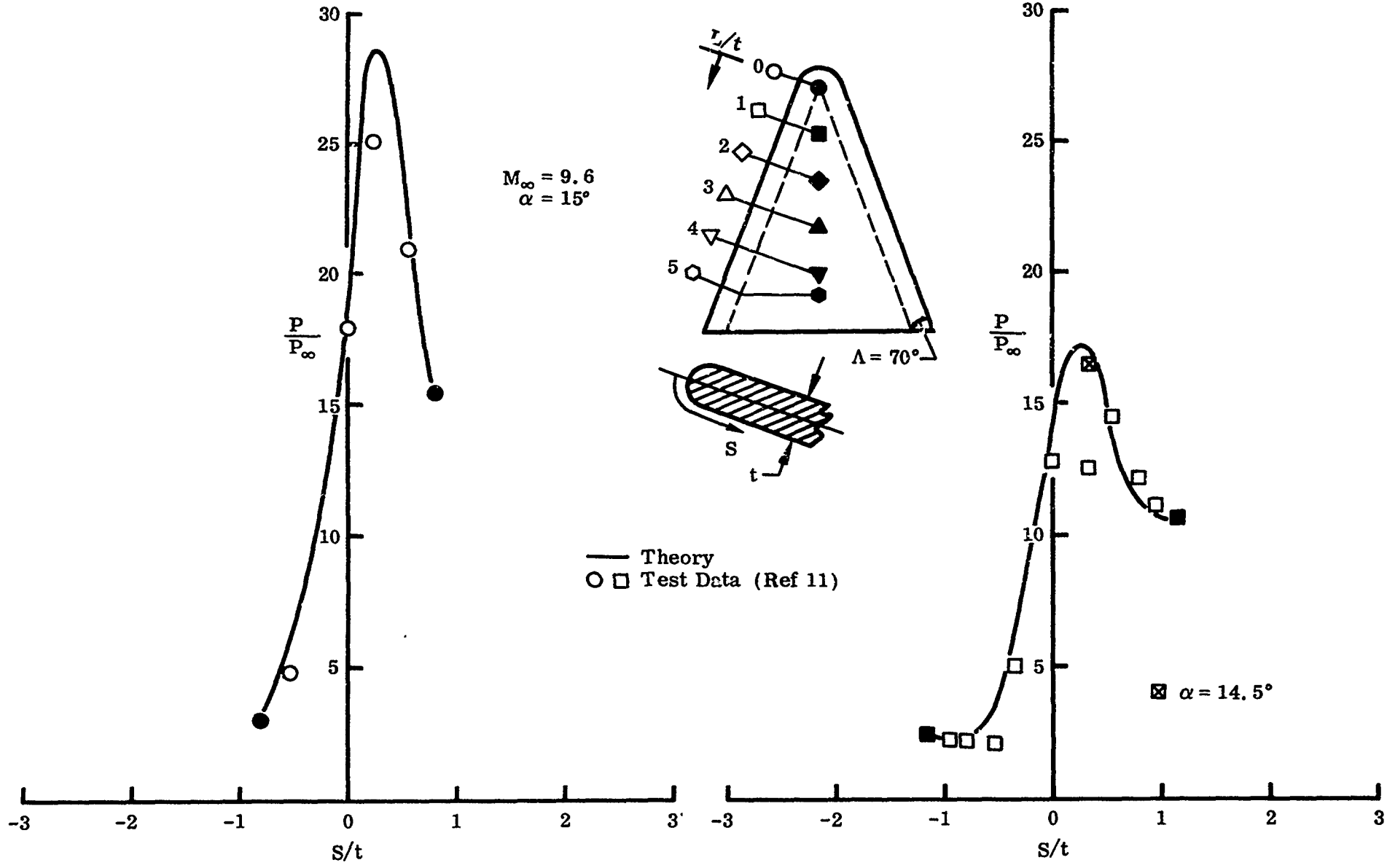

(a) Station L/t = 0

(b) Station L/t = 1

FIGURE 30. PRESSURE DISTRIBUTION NORMAL TO THE LEADING EDGE ON A SPHERICALLY-NOSED SLAB DELTA WING WITH 70° SWEEP

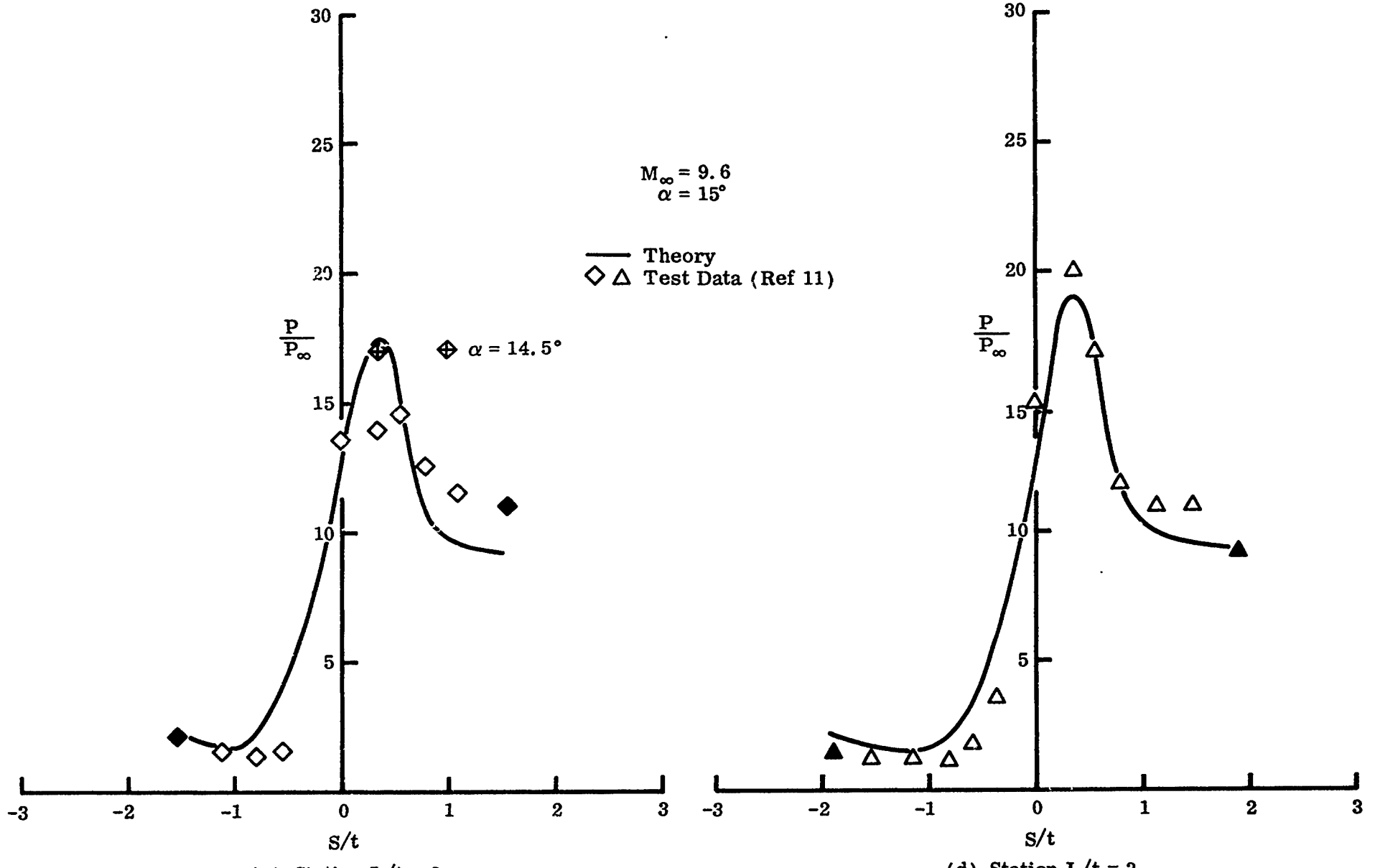

(c) Station L/t = 2

(d) Station L/t = 3

FIGURE 30. (Continued)

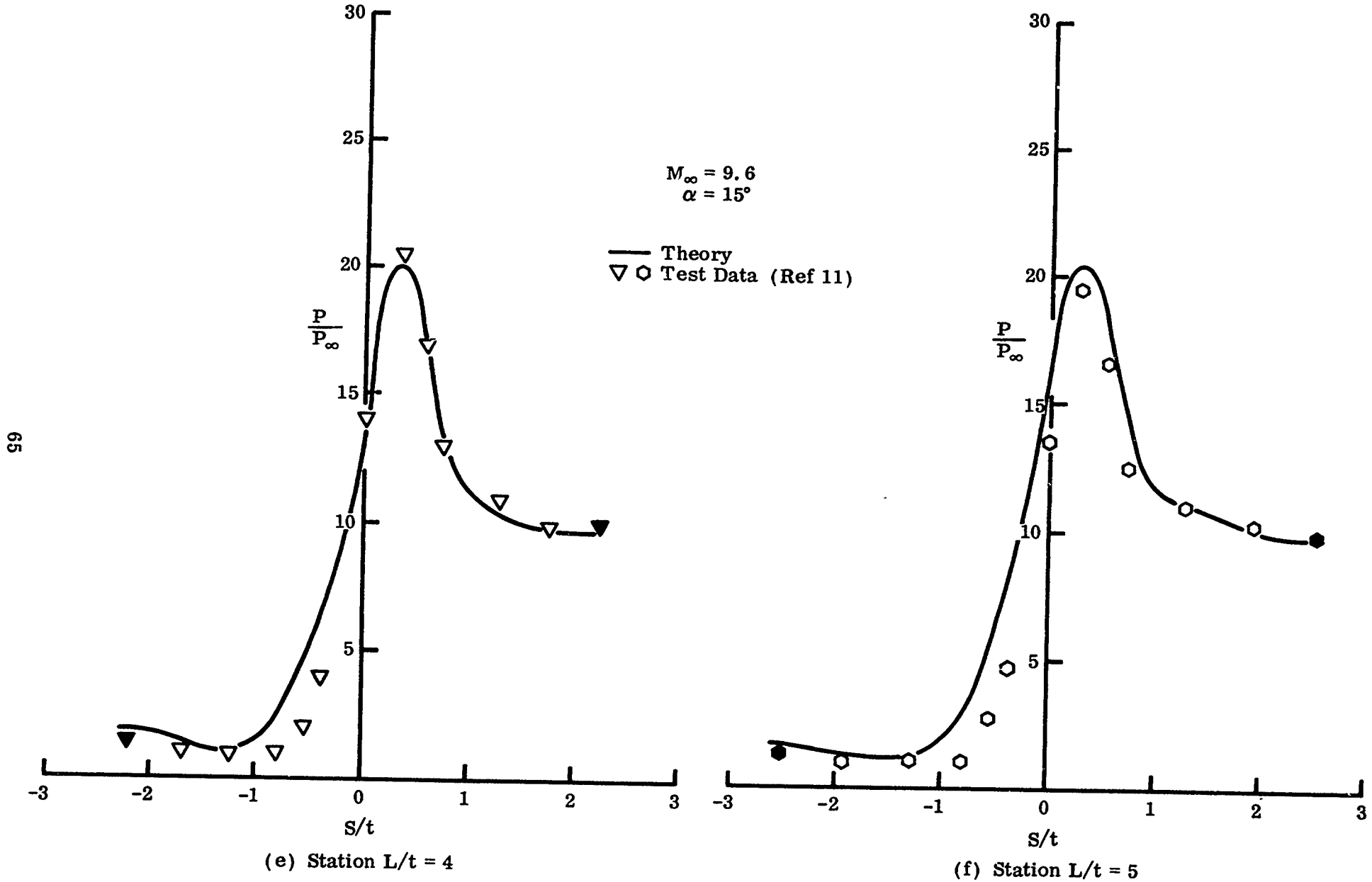

(e) Station L/t = 4

(f) Station L/t = 5

FIGURE 30. (Concluded)

SECTION VI

CONCLUSION

A new version of the three-dimensional method of characteristics has been developed to calculate the steady supersonic inviscid flow around smooth three-dimensional bodies at general angles of attack. Many new approaches and procedures have been devised and incorporated to improve the numerical method and the computer program. Flow fields over various body shapes under different freestream conditions have been calculated. The computed results were compared with available experimental data with good agreement as exemplified by the two test cases presented in this report.

It has been proven that the new three-dimensional method of characteristics, which is efficient, accurate, and versatile, is an important tool for flow field analysis and vehicle design. Possible extensions include the treatment of bodies with surface slope discontinuities, such as the compression or expansion corners, and the calculation of embedded shocks resulting from fins and canopies. The basic schemes for calculating the embedded shocks have been conceived and are ready for development.

REFERENCES

1. Powers, S. A., et al, "A Numerical Procedure for Determining the Combined Viscid-Inviscid Flow Fields Over Generalized Three-Dimensional Bodies," AFFDL-TR-67-124, Vol. I, 1967.

2. Van Dyke, M. D. and Helen D. Gordon, "Supersonic Flow Past a Family of Axisymmetric Bodies," NASA TR R-1, 1959.

3. Powers, S. A. and J. B. O'Neill, "Determination of Hypersonic Flow Fields by the Method of Characteristics," AIAA Journal, Vol. 1, No. 7, July 1963, pp. 1963-4.

4. Sears, W. R. (editor), General Theory of High Speed Aerodynamics, Princeton University Press, Princeton, New Jersey, 1954.

5. Chu, C. W., "A New Algorithm for Three-Dimensional Method of Characteristics," (to be published in AIAA Journal).

6. Chu, C. W., "Calculation of Steady Three-Dimensional Supersonic Flow About Fuselages," Northrop Corporation Report NOR 70-150, 1972.

7. Chu, C. W., "A Simple Derivation of Three-Dimensional Characteristic Relations," AIAA Journal, Vol. 2, No. 7, July 1964, pp. 1336-7.

8. Chu, C. W., "Compatibility Relations and a Generalized Finite-Difference Approximation for Three-Dimensional Supersonic Flow," AIAA Journal, Vol. 5, No. 3, March 1967, pp. 493-501.

9. Cleary, J.W. and C. E. Duller, "Effects of Angle of Attack and Bluntness on the Hypersonic Flow Over a 15° Semiapex Cone in Helium," NASA TN D-5903, 1970.

10. Rakich, J. V. and J. W. Cleary, "Theoretical and Experimental Study of Supersonic Steady Flow Around Inclined Bodies of Revolution," AIAA paper 69-187, 7th Aerospace Sciences Meeting, January 20-22, 1969.

11. Bertram, M. H. and P. E. Everhart, "An Experimental Study of the Pressure and Heat Transfer Distribution on a 70° Sweep Slab Delta Wing in Hypersonic Flow," NASA TR R-153, 1963.

APPENDIX I

EVALUATION OF THE COEFFICIENTS FOR A CONIC SECTION

The general equation of a conic is

$$aY^2 + bXY + cX^2 + dY + eX + f = 0 \tag{1}$$

This can be arranged into a more suitable form

$$Y = PX + Q \pm \sqrt{RX^2 + SX + T} \tag{2}$$

By factoring Equation (1), the following combination of linear equations can be derived:

$$K(Y - m_1X - h_1)(Y - m_3X - h_3) + (Y - m_2X - h_2)(Y - m_4X - h_4) = 0 \tag{3}$$

where m_1, m_2, ---, h_4, and K are constants to be evaluated. Note that Equation (2) has five coefficients. Thus, a general conic can be passed through any five points not lying on a straight line; in some cases the results will be two branches of a hyperbola. Therefore, given five points in a plane, as shown in the sketch below, the first four can be connected by straight lines. These lines are defined by the slopes, m_i, and the constants, h_i, and these are evaluated using the ordinates and abscissas of the four points.

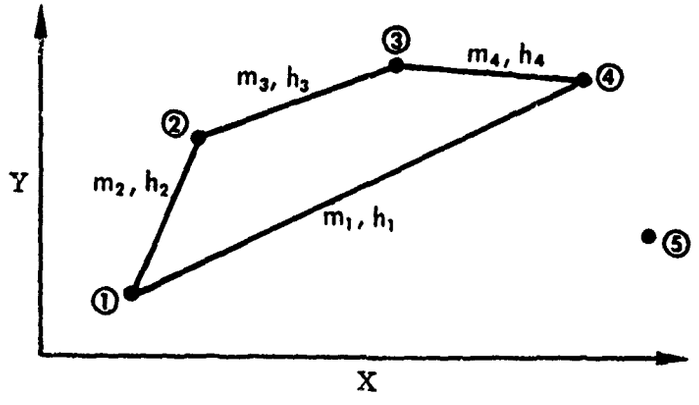

If point 1 is substituted into Equation (3), the result is identically zero, since point 1 was used to evaluate the coefficients m_1, h_1, m_2, and h_2. The same argument holds for point 2, 3, and 4.

The value of K can be established by evaluating Equation (3) at point 5 to obtain the following result

$$K = -\frac{(Y_5 - m_2X_5 - h_2)(Y_5 - m_4X_5 - h_4)}{(Y_5 - m_1X_5 - h_1)(Y_5 - m_3X_5 - h_3)}$$

By expanding Equation (3) and collecting like powers, it can be shown that

$$P = -B/2A$$

$$Q = -D/2A$$

$$R = P^2 - C/A$$

$$S = -PD/A - E/A$$

$$T = Q^2 - F/A$$

where

$$A = K + 1$$

$$B = -[K(m_1 + m_3) + m_2 + m_4]$$

$$C = Km_1m_3 + m_2m_4$$

$$D = -[K(h_1 + h_3) + h_2 + h_4]$$

$$E = K(m_1h_3 + m_3h_1) + m_2h_4 + m_4h_2$$

$$F = Kh_1h_3 + h_2h_4$$

and the sign of the radical must be determined by evaluation.

To determine the coefficients when four points and one slope are given, let the location of points 1 and 2 coincide, with m_2 being the given slope. The remainder of the analysis follows identically.

For three points and two slopes, let points 1 and 2 coincide and points 3 and 4 coincide, with the given slopes being m_2 and m_4. The rest of the analysis is the same.

Two special forms are worth noting:

A straight line has the coefficients

P = slope

Q = constant

$R = S = T = 0$

A circle with its center at the point (X_0, Y_0), has the coefficients

$P = 0$

$Q = X_0$

$R = -1$

$S = 2Y_0$

$T = R^2 - Y_0^2$

APPENDIX II

SAMPLE BODY DESCRIPTIONS

1. SLAB DELTA WING WITH 70° SWEEP

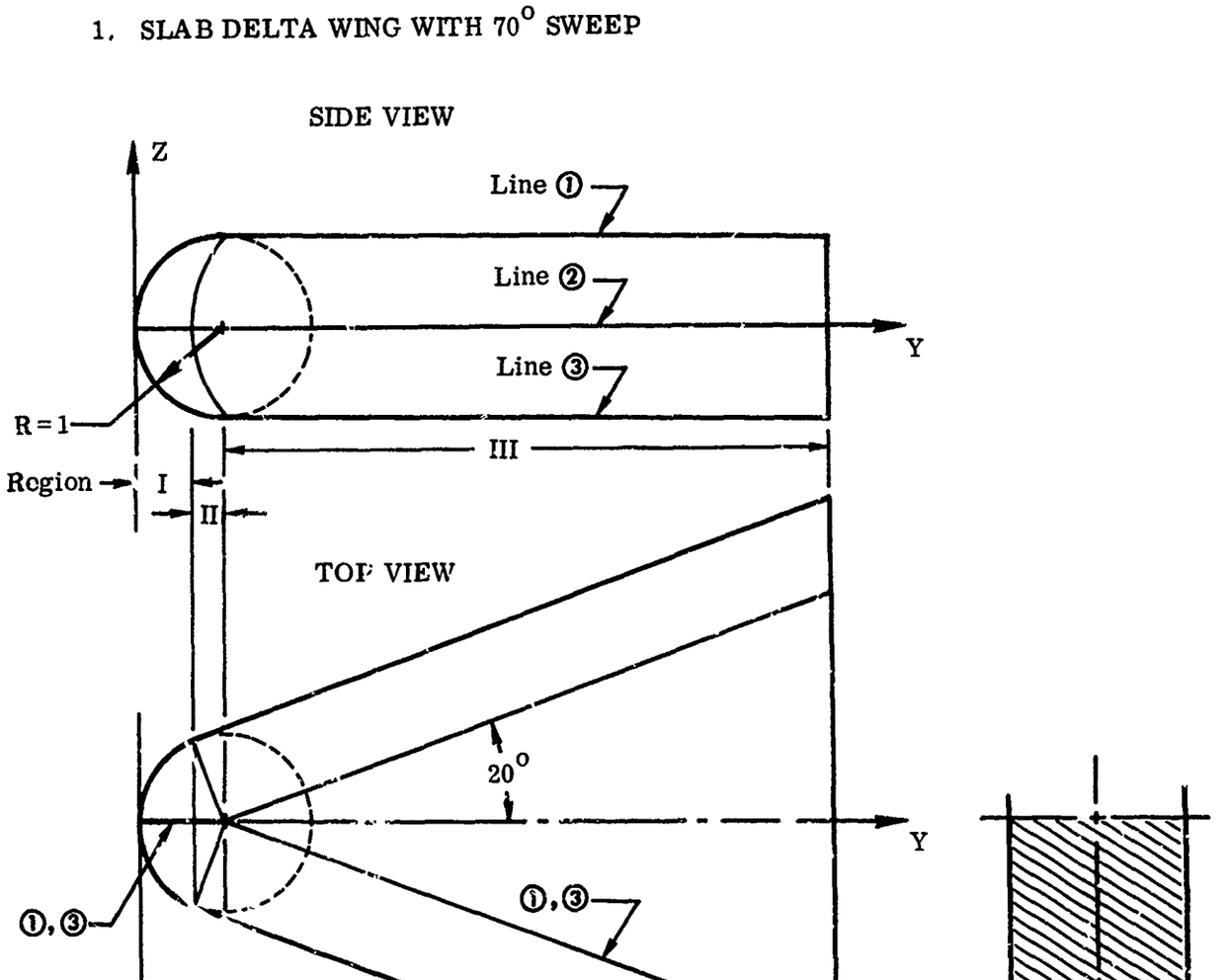

LINE ①

- Regions I and II : $0 \leq Y < 1$

$$Z_1 = \sqrt{-Y^2 + 2Y}$$
$$X_1 = 0$$

- Region III : $1 \leq Y \leq 7$

$$Z_1 = 1$$
$$X_1 = (\tan 20^\circ)Y + (-\tan 20^\circ)$$

LINE ②

- Region I : $0 \leq Y < (1 - \sin 20^\circ)$

$$Z_2 = 0$$
$$X_2 = \sqrt{-Y^2 + 2Y}$$

- Regions II and III : $(1 - \sin 20^\circ) \leq Y \leq 7$

$$Z_2 = 0$$
$$X_2 = (\tan 20^\circ)Y + (\cos 20^\circ - \tan 20^\circ + \tan 20^\circ \sin 20^\circ)$$

LINE ③

- Regions I and II : $0 \leq Y < 1$

$$Z_3 = -\sqrt{-Y^2 + 2Y}$$
$$X_3 = 0$$

- Region III : $1 \leq Y \leq 7$

$$Z_3 = -1$$
$$X_3 = (\tan 20^\circ)Y + (-\tan 20^\circ)$$

Thus, the coefficients P, Q, R, S, and T are as follows :

- Region I : $0 \leq Y < (1 - \sin 20^{\circ})$

$P_1 = 0$	$Q_1 = 0$	$R_1 = -1$	$S_1 = 2$	$T_1 = 0$	$SG_1 = +1$
$P_2 = 0$	$Q_2 = 0$	$R_2 = 0$	$S_2 = 0$	$T_2 = 1$	$SG_2 = 0$[4]
$P_3 = 0$	$Q_3 = 0$	$R_3 = -1$	$S_3 = 2$	$T_3 = 0$	$SG_3 = -1$
$P_4 = 0$	$Q_4 = 0$	$R_4 = 0$	$S_4 = 0$	$T_4 = 1$	$SG_4 = 0$
$P_5 = 0$	$Q_5 = 0$	$R_5 = 0$	$S_5 = 0$	$T_5 = 1$	$SG_5 = 0$
$P_6 = 0$	$Q_6 = 0$	$R_6 = 0$	$S_6 = 0$	$T_6 = 1$	$SG_6 = 0$

- Region II : $(1 - \sin 20^{\circ}) \leq Y < 1$

change to the following

$P_5 = (\tan 20^{\circ})$ $Q_5 = (\cos 20^{\circ} - \tan 20^{\circ} + \tan 20^{\circ} \sin 20^{\circ})$

$R_5 = 0$ $S_5 = 0$ $T_5 = 1$ $SG_5 = 0$

- Region III : $1 \leq Y \leq 7$

change to the following

$P_1 = 0$	$Q_1 = 1$	$R_1 = 0$	$S_1 = 0$	$T_1 = 1$	$SG_1 = 0$
$P_3 = 0$	$Q_3 = 1$	$R_3 = 0$	$S_3 = 0$	$T_3 = 1$	$SG_3 = 0$
$P_4 = (\tan 20^{\circ})$	$Q_4 = (-\tan 20^{\circ})$	$R_4 = 0$	$S_4 = 0$	$T_4 = 1$	$SG_4 = 0$
$P_6 = (\tan 20^{\circ})$	$Q_6 = (-\tan 20^{\circ})$	$R_6 = 0$	$S_6 = 0$	$T_6 = 1$	$SG_6 = 0$

[4] When the numerical value of the square root is identically zero, it is best to assign +1 to T and 0 to SG, so that the SQRT function will not generate an error message.

2. BLUNTED 15^{O} CONE

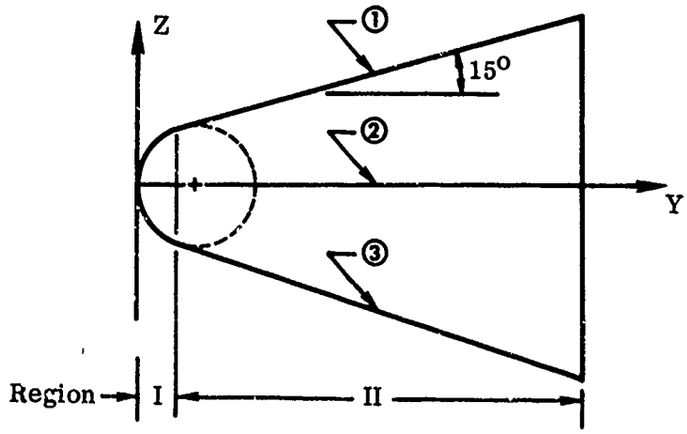

SIDE VIEW

Note that for the blunted cone, lines ① and ③ both lie in the plane of symmetry.

LINE ①

- Region I : $0 \leq Y < (1 - \sin 15^{O})$

$$Z_1 = \sqrt{-Y^2 + 2Y}$$

$$X_1 = 0$$

- Region II : $(1 - \sin 15^{O}) \leq Y \leq 5$

$$Z_1 = (\tan 15°)Y + (\cos 15° - \tan 15° + \tan 15° \sin 15°)$$

$$X_1 = 0$$

LINE ②

- Region I : $0 \leq Y < (1 - \sin 15^{O})$

$$Z_2 = 0$$

$$X_2 = \sqrt{-Y^2 + 2Y}$$

• Region II : $(1-\sin 15^{0}) \leq Y \leq 5$

$$Z_2 = 0$$

$$X_2 = (\tan 15°)Y + (\cos 15° - \tan 15° + \tan 15° \sin 15°)$$

LINE ③

• Region I : $0 \leq Y < (1-\sin 15^{0})$

$$Z_3 = -\sqrt{-Y^2+2Y}$$

$$X_3 = 0$$

• Region II : $(1-\sin 15^{0}) \leq Y \leq 5$

$$Z_3 = (-\tan 15°)Y - (\cos 15° - \tan 15° + \tan 15° \sin 15°)$$

$$X_3 = 0$$

Thus, the coefficients P, Q, R, S, and T are as follows:

• Region I : $0 \leq Y < (1-\sin 15^{0})$

$P_1 = 0$	$Q_1 = 0$	$R_1 = -1$	$S_1 = 2$	$T_1 = 0$	$SG_1 = +1$
$P_2 = 0$	$Q_2 = 0$	$R_2 = 0$	$S_2 = 0$	$T_2 = 1$	$SG_2 = 0$
$P_3 = 0$	$Q_3 = 0$	$R_3 = -1$	$S_3 = 2$	$T_3 = 0$	$SG_3 = -1$
$P_4 = 0$	$Q_4 = 0$	$R_4 = 0$	$S_4 = 0$	$T_4 = 1$	$SG_4 = 0$
$P_5 = 0$	$Q_5 = 0$	$R_5 = -1$	$S_5 = 2$	$T_5 = 1$	$SG_5 = +1$
$P_6 = 0$	$Q_6 = 0$	$R_6 = 0$	$S_6 = 0$	$T_6 = 1$	$SG_6 = 0$

• Region II : $(1-\sin 15^{0}) \leq Y \leq 5$

change to the following

$P_1 = (\tan 15°)$ $Q_1 = (\cos 15° - \tan 15° + \tan 15° \sin 15°)$

$R_1 = 0$ $S_1 = 0$ $T_1 = 1$ $SG_1 = 0$

$P_3 = (-\tan 15°)$ $Q_3 = -(\cos 15° - \tan 15° + \tan 15° \sin 15°)$

$R_3 = 0$ $S_3 = 0$ $T_3 = 1$ $SG_3 = 0$

$P_5 = (\tan 15°)$ $Q_5 = (\cos 15° - \tan 15° + \tan 15° \sin 15°)$

$R_5 = 0$ $S_5 = 0$ $T_5 = 1$ $SG_5 = 0$